Geofísica Internacional (2015) 54-3: 221-244

Original paper

Mesozoic gliding and Tertiary basin and range tectonics in eastern Sonora, Mexico

José Luis Rodríguez Castañeda, Jaime Roldán Quintana and Amabel Ortega Rivera

Received: August, 06, 2013; accepted: August 27, 2014; published on line: June 30, 2015

DOI: 10.1016/j.gi.2015.04.018

Resumen

En el oriente de Sonora, México, se encuentran bien preservadas en rocas del Cretácico Superior de la región de Arivechi, estructuras de deformación compleja asociadas a movimientos verticales y actividad gravitacional como deslizamientos. Estas estructuras nos permitieron hacer la distinción entre estructuras de origen sin-sedimentario y de origen tectónico. Las rocas en Arivechi, de acuerdo con su litología y grado de deformación, se dividieron en dos unidades la Unidad Cañada de Tarachi (la más antigua) y la Unidad El Potrero Grande. La secuencia volcano-sedimentaria del Cretácico Superior tiene más de 6 km de espesor y consiste en una secuencia de toba riolítica, andesita, conglomerado, arenisca, limolita y lutita que fueron depositadas en la cuenca tras arco de Arivechi. Dentro de la Unidad Cañada de Tarachi se encontraron monolitos y bloques que son los que constituyen uno de los objetivos principales de esta investigación. La edad de los monolitos y bloques incluyen rocas del Proterozoico, Paleozoico y Mesozoico. Los monolitos del Proterozoico están dominados por arenisca de cuarzo y dolomía. Los monolitos del Paleozoico y Mesozoico consisten en caliza y lutita interestratificadas, conglomerado y roca ígnea. Dos de los bloques graníticos fueron fechados; uno de ellos en 76 Ma (edad U/Pb en zircón) y el segundo en 70 Ma ($^{40}Ar/^{39}Ar$ roca total por calentamiento a pasos). Los monolitos sedimentarios muestran una transición gradacional desde capas coherentes en sus porciones superior y media, a una intensa deformación en sus bordes y bases. Las estructuras dentro de los megaclastos y bloques, así como las rocas que los rodean, se estudiaron a detalle, para reconstruir el origen y desarrollo estructural de los monolitos, bloques y rocas encajonantes. La nueva información estratigráfica y estructural nos permite inferir que la posible fuente de los monolitos y bloques fue una tierra positiva localizada hacia el oriente de Arivechi en el oeste de Chihuahua y oriente de Sonora, México, denominada la Plataforma de Aldama. Las estructuras identificadas consisten en pliegues y fallas normales. La vergencia de los pliegues sugiere que el depocentro estaba localizado hacia el oeste del área de estudio.
Se efectuó una reconstrucción de paleoesfuerzos con el fin de documentar la historia tectónica del margen oriental de la posible cuenca de tras-arco de Arivechi. Se utilizó el método de inversión de esfuerzos a partir de los datos de deslizamiento de las fallas aplicando el método *right-dihedra* mejorado, seguido por una optimización rotacional. El análisis estructural y la reconstrucción de esfuerzos muestran que la evolución cinemática Mesozoico-Cenozoico se caracterizó por extensión. Este régimen continuó después del Cretácico y ha sido identificado en el Mioceno. La secuencia de rocas fue modificada por una deformación Cenozoica tipo Cuencas y Sierras, caracterizada por fallamiento normal durante el Mioceno, como sugiere la reconstrucción de los paleoesfuerzos. Este último evento fue el resultado del cambio del régimen tectónico, de subducción de la placa Farallón al régimen de fallamiento transcurrente que da inicio al sistema de fallas San Andres-Golfo de California durante el Mioceno. La cronología de eventos identificados sugiere que la dirección de extensión NE-SW y ENE-WSW fueron seguidos por extensión E-W y WNW-ESE. Esto indicaría que la secuencia del fallamiento fue de NE-SW a ENE-WSW y, por último, a WNW-ESE.

Palabras clave: Tectónica por gravedad, Cretácico Superior, monolitos, bloques, deslizamiento por gravedad, paleo esfuerzos, Sonora.

J. L. Rodríguez Castañeda*
J. Roldán Quintana
A. Ortega Rivera
Estación Regional del Noroeste
Instituto de Geología
Universidad Nacional Autónoma de México

Blvd. Luis Donaldo Colosio y Madrid, CP 83000,
Hermosillo, Sonora
México
Corresponding author: jlrod@unam.mx

Abstract

Complex deformational structures assigned to vertical movements, and gravitational activity, such as gliding, are well preserved in Upper Cretaceous rocks of the Arivechi region, Eastern Sonora, Mexico. These structures allow us to discriminate between synsedimentary and tectonic origins. The rocks at Arivechi have been divided into two units according to their lithology and degree of deformation, the Cañada de Tarachi (oldest) and El Potrero Grande units. The Upper Cretaceous volcano-sedimentary sequence is more than 6 km thick and consists mainly of andesite, rhyolithic tuff, conglomerate sandstone, siltstone, and shale-type rocks that were deposited in the Arivechi back-arc basin. Within the Cañada de Tarachi Unit, monoliths and blocks were found; these include rocks dating from Proterozoic, Paleozoic and Mesozoic times. The Proterozoic monoliths are dominated by quartz sandstone and dolomite and the Paleozoic and Mesozoic monoliths consist of limestone, shale, limestone-shale-sandstone, conglomerate and igneous rocks. Two granitic monoliths have been dated, one at 76 Ma (U/Pb zircon date) and the other at 70 Ma ($^{40}Ar/^{39}Ar$ whole rock step-heating). The sedimentary monoliths show gradational transitions from coherent beds to intense deformation along their edges and bases. The structure within the monoliths, blocks and surrounding host rocks was studied in detail. The new stratigraphic and structural data suggest that the monoliths and blocks may have originated at a positive land east of Arivechi, in western Chihuahua and eastern Sonora, Mexico, known as the Aldama Platform. The identified structures consist of folds and normal faults. Fold vergence suggests that the depocenter was located westward of the study area. A paleostress reconstruction documented the tectonic history of the eastern margin of the Arivechi back-arc basin. Stress inversion of fault slip data was achieved by an improved right-dihedra method followed by rotational optimization. The structural analysis and paleostress reconstructions showed that the Mesozoic-Cenozoic kinematic evolution was extensional and continued during Cretaceous times; it has also been identified in Miocene rocks. The rock sequence was modified by basin and range-type normal faulting, as suggested by our paleostress reconstruction. The last event is the result of the beginning of tectonic extension at the onset of the shift from a subduction regime toward a transform fault regime, i.e., from the subduction of the Fallaron plate to the San Andreas Gulf of California fault system during Miocene times. NE-SW and ENE-WSW extension was followed by E-W and WNW-ESE extension. The faulting sequence went from NE-SW to ENE-WSW and subsequently to WNW-ESE.

Key Words: Gravity tectonics, Upper Cretaceous monoliths, blocks, gravity gliding, paleostress, Sonora.

Introduction

The active margin of western North America, which encompasses eastern Sonora, is characterized by the development of extensive and thick Upper Cretaceous rocks units (Figure 1). It has been generally accepted that Upper Cretaceous deformation in eastern Sonora is associated with the compressional Laramide orogeny, characterized by the fold and thrust belt in the western United States. However, new studies in north-eastern Sonora suggest that compressional structures are related to gravitational gliding rather than thrusting and folding by tectonic compression. Gliding tectonics is a mechanism whereby large masses of rocks move down a slope under gravity, producing folding and faulting of varying extent and complexity (Allaby and Allaby, 1999).

The Arivechi region was selected for better understanding of the evolution of these structures in eastern Sonora. Previous studies have reported that Upper Cretaceous rocks exist and that deformation is related to tectonic compression (Fernández-Aguirre and Almazán-Vázquez, 1991; Fernández-Aguirre *et al*., 1995; Minjárez-Sosa *et al*., 1985; Palafox *et al*., 1984; Palafox and Martínez, 1985). A detailed stratigraphic, morphostructural integration with structural analysis of fragile and ductile mesostructures present in the Upper Cretaceous rocks, paleostress analysis, and geochronological studies were conducted in order to ascertain whether the structures were originated by extension or compression.

Geological framework

Our study area, located east of Arivechi, has been subjected to several studies of stratigraphy and paleontology and, to a lesser extent, structural geology. We defined two units of Mesozoic age: 1) Cañada de Tarachi Unit, and 2) El Potrero Grande Unit. A third unit is of Oligocene-Miocene age, the Sierra Madre Occidental volcanic sequence. The two Upper Cretaceous units constitute

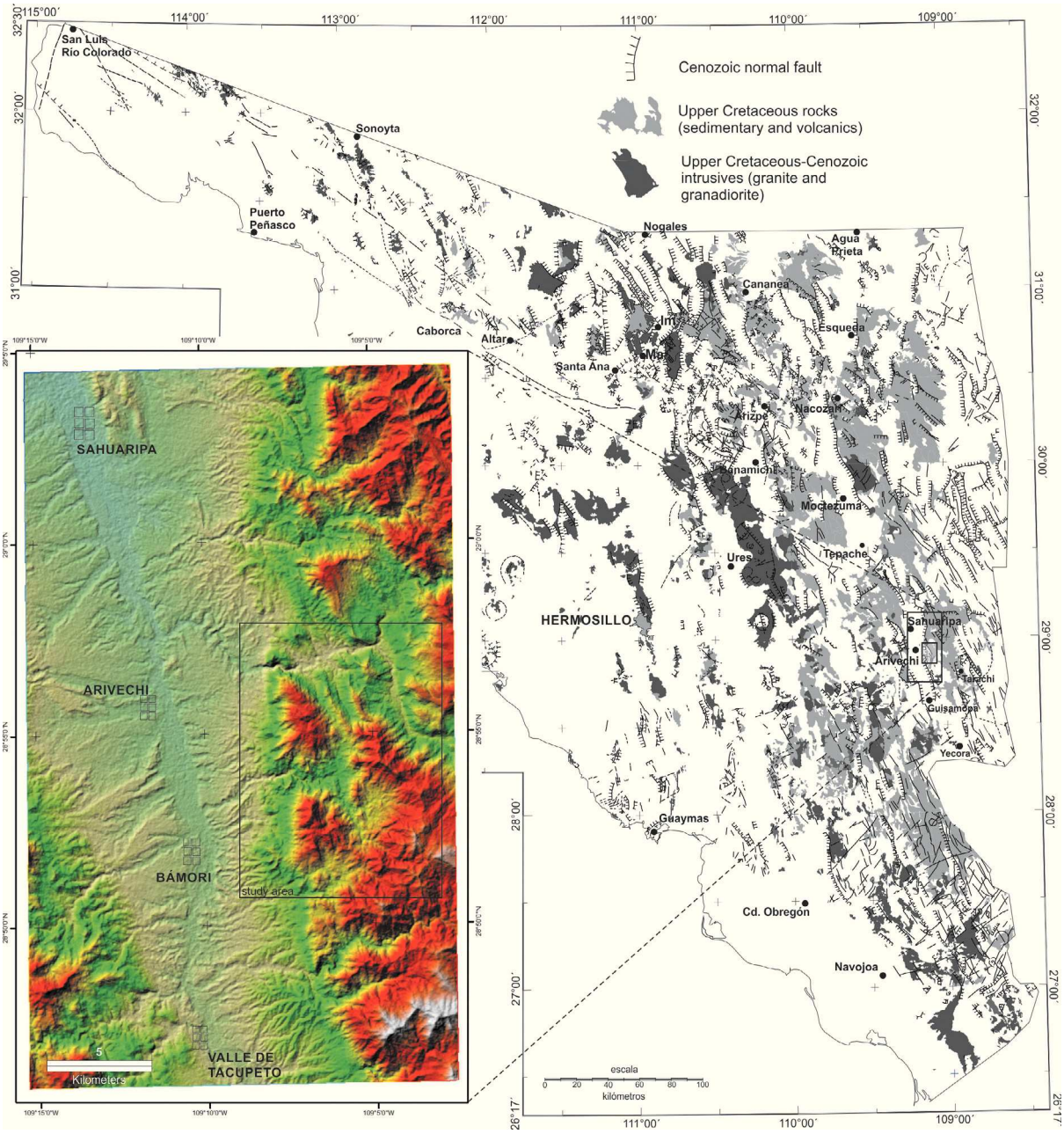

Figure 1. Location of the Arivechi region in eastern Sonora, Mexico and its relationship with the Upper Cretaceous rocks. Geologic information from the Servicio Geológico Mexicano (2008).

a volcano-sedimentary sequence of more than 6 km thickness. El Potrero Grande Unit (the youngest Cretaceous sequence) consists of conglomerate, sandstone, siltstone, and shale with interbedded andesite and diorite dikes and layers of rhyolitic tuffs. These rocks constitude a column more than 2,400 m thick, but this is merly part of a thicker sequence. The oldest unite include a large number of unusually well-exposed megaclasts of different lithogies and ages. A megaclast is a term used in grain-size schemes after modification of the Udden-Wentworth sedimentary grain-size scale devised by Blair and McPherson (1999), who proposed a new fraction in sediment size to account for clasts larger than 4.1m. They proposed four sizes for the megaclast fraction: *block* (4.1 to 65.5 m), *slab* (65.5 to 1049 m), *monolith* (1 to 33.6 km), and *megalith* (d_I from 33.6 to 1075 km). Megaclasts are associated to gravity sliding, or to vertical movements as described by various authors as olistoliths and olistostromes (Teale and Young, 1987; Heubeck, 1992).

Megaclasts have also been reported from numerous other tectonic environments; the Pyrenées (Johns *et al*., 1981), the Canadian Rockies (Cook *et al*., 1972), eastern Australia (Conaghan *et al*., 1976), the western US Cordillera (Heck and Speed 1987), the Apennines (Naylor, 1982; Teale and Young, 1987), the Avalonían Terrane of New England (Bailey *et al*., 1989), Hispaniola (Heubeck, 1992), global recent continental slopes (Prior *et al*., 1982), Alaska (Harp *et al*., 2003), the Valles-San Luis Potosi Platform (Carrasco-Velázquez., 1977), and north-eastern Sonora (McKee and Anderson, 1998; McKee *et al*., 2005).

Megaclasts (monoliths and blocks) as described by Blair and McPherson (1999), have been found and are common in eastern Sonora Upper Cretaceous sequences (McKee and Anderson, 1998; Rodríguez-Castañeda, 2002; and McKee *et al*. 2005). These megaclasts have been linked to the emergence of a positive land, possibly related to the Late Jurassic Aldama Platform (Ramirez and Acevedo, 1957; Monreal, 1996; Haenggi, 2002; Anderson and Nourse, 2005) (Figure 2). The Aldama Platform is defined as an emerged land oriented NW-SE in north-west Chihuahua and eastern Sonora. Its extension toward north-eastern Sonora could be the Cananea High (McKee, 1991; Rodríguez-Castañeda, 2002). The Aldama Platform is bounded by faults related to the platform uplift. Uplift has been suggested as a mechanism of megaclast generation. It has been attributed to different causes but mainly to extension by reactivation of old faults and early Cenozoic pluton emplacement (Rodríguez-Castañeda,

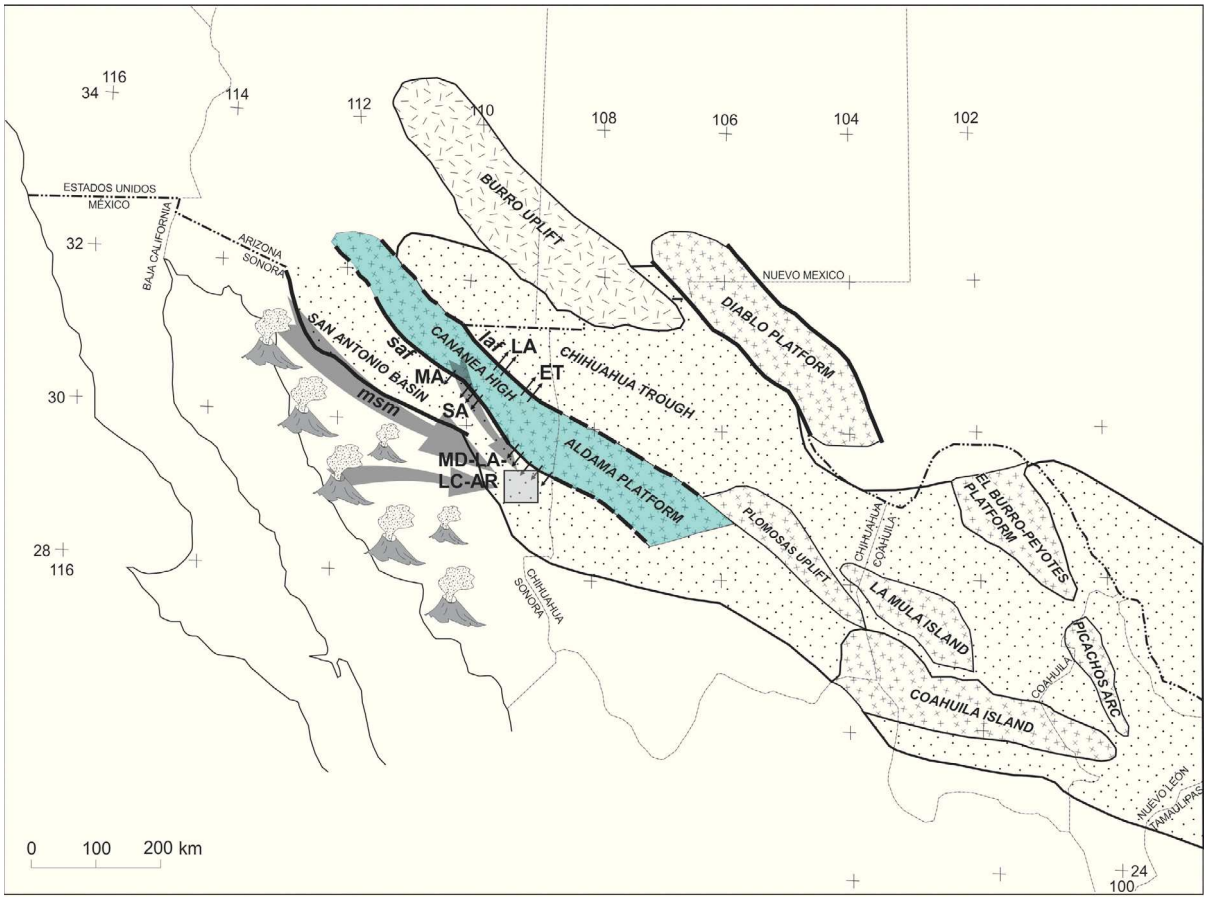

Figure 2. Map showing the paleogeography and structural elements that controlled the geologic evolution in the Upper Cretaceous. The Aldama Platform and its possible continuation towards the north-east of Sonora as the Cananea High were important elements in the evolution of the study area. The black arrows show the occurrence of slipped megaclasts and the gray arrows suggest the possible source of the sediments that constitute the rocky outcrops of the Upper Cretaceous in the study area (square). Megaclast localities: Los Ajos (LA), El Tigre (ET), Magdalena (MA), San Antonio (SA), La Madera (MD), Lampazos (LA), Los Chinos (LC) and Arivechi (AR), *msm* = Mojave-Sonora megashear, *saf* = San Antonio fault, *laf*= Los Ajos fault. Modified from Anderson and Nourse (2005) including Monreal (1996).

2002; Roldán-Quintana, 2002). Epiclastic, pyroclastic and reworked deposits have also been identified in the study area. Flows and pyroclastic rock falls, mass waste deposits and volcaniclastic turbidites are common in the sequence deposited in the Arivechi back-arc basin. Towards the top of the unit the finest sediments increase in proportion, marking the latest stage of the evolution of this type of basin (Spalletti, 2006).

Regional Geology

Although several studies have been carried out knowledge of Mesozoic geology in the Arivechi-Sahuaripa region is still sketchy. King (1939), Himanga (1977), Flinn (1977), Palafox and Martínez (1985), Minjarez *et al*. (1985), Pubellier (1987), and Fernández-Aguirre and Almazán-Vázquez (1991), among others, mainly focused on stratigraphic relationships; however, they also provide descriptions of structural.

Some of these descriptions are as follows: at Sierra El Chiltepín, 20 km north-west of Arivechi, Himanga (1977) described a fold and a thrust with a NW-SE orientation as a result of a NE-SW compression. In the Cerro Macho area, west of Arivechi, Flinn (1977) reported the existence of an exotic Lower Cretaceous thrusting over Upper Cretaceous-Paleogene rocks. Stewart *et al*. (2002) described Proterozoic (700 Ma) sedimentary rocks at Sierra El Chiltepín consisting of well-cemented quartz sandstone intercalated with limestone containing stromatolites, which thrust eastward over Lower Cretaceous rocks.

Also, south of Sierra Chiltepín, at Cerros La Sata and El Mogallón, located 9 km west of Arivechi, Almazán-Vázquez (1989) reported a package of Cambrian and Ordovician sedimentary rocks which are strongly dislocated by normal faults. He also reported outcrops of rocks of Jurassic and Cretaceous age similar to those exposed in the area of Arivechi.

On the other hand, in the Lampazos area, 40 km north-east of Arivechi, Herrera and Bartolini (1993) and González-León (1988) reported Laramidic structures in Lower Cretaceous rocks which consisted of parallel folds with north-east vergence, NW-SE reverse faults and overthrust faults. Bartolini (1993) suggested that the Cretaceous rocks of the Lampazos area correspond to isolated platform fragments with no genetic connection with the sequences exposed in central and northern Sonora. He suggested that in eastern Sonora Lower Cretaceous blocks relate to parts of the Aldama Platform in central Chihuahua and that they slide westward along a NW-facing slope.

East of Arivechi, at Cerros Las Conchas and El Palmar, King (1939) observed that Paleozoic rock slivers could be found on top of Cretaceous rocks, and Palafox and Martínez (1985) and Fernández-Aguirre and Almazán-Vázquez (1991) noted that the deformation of the Laramide Orogeny in the area of Arivechi is represented by tight folds, thrusts and small reverse faults. Minjarez-Sosa *et al*. (1985) believe the folds and reverse faults are the result of the Albian-Cenomanian deformation, as reported by Rangin (1977, 1982).

Likewise, Pubellier (1987) reported the presence of four deformational events in the Sahuaripa and Arivechi region: a Jurassic event responsible for the deposit of coarse clasts; a tectonic phase assigned to the Late Albian-Late Santonian that carried rock fragments of Proterozoic basement on top of Lower Cretaceous rocks with transport N-NE; the Laramide orogeny in the Paleocene, which folded the structures of the previous event with a south-westerly vergence trend which in turn were cut by intrusive rocks during the lower Eocene, and, finally, two extensional events expanding from the Miocene to the present, creating normal faulting.

In the Lampazos area, north of Sahuaripa, the Cretaceous sequence may be lithologically correlated with western Chihuahua Lower Cretaceous rocks (Monreal, 1995). The Cretaceous rocks exposed in Lampazos and Sierra Los Chinos represent basin facies, whereas Lower Cretaceous rock facies, in Sonora, are platform facies (Monreal and Longoria, 2000). According to González-León (1988), there are differences between the facies of these rocks and the Bisbee group; the rocks of Lampazos rather resemble rocks of the same age as those of Chihuahua.

Lastly, at Sierra Los Chinos, 30 km north of Sahuaripa, Monreal and Longoria (2000) and Díaz and Monreal (2008) concluded from the microfossil content that this area encompasses Lower Cretaceous rocks that correspond to the Chihuahua basin or to gradational facies between this basin and the Bisbee Basin.

Methodology

For better understanding and constraining of the sequence of geological events in the Arivechi region, geological mapping was conducted at a scale of 1:25,000. We also aimed to complete stratigraphic measurements and descriptions

of the lithology; measure and analyze the structural data obtained in the field; obtain paleostress tensors; construct the kinematics and paleostress evolution of the Arivechi area; determine the structural effects in the basin evolution; and discuss the implications of our results regarding the tectonic evolution of eastern Sonora. U/Pb zircon and $^{40}Ar/^{39}Ar$ geochronology was conducted for two selected rock samples.

U/Pb Method

The geochronology was carried out at the Centro de Geociencias Isotopic lab, UNAM. The method of dating is as follows. Laser ablation inductively-coupled plasma mass spectrometry (LA-ICPMS) U-Pb analyses were performed at the Laboratorio de Estudios Isotópicos (LEI), Centro de Geociencias, UNAM, employing a 193 nm excimer laser workstation (Resolution M-050) coupled with a Thermo X-ii quadrupole ICPMS. The protocol reported by Solari *et al*. (2010) was used, employing a 23 μm analytical spot and the Plešovice zircon (Slama *et al*., 2008) as bracketing standard. Time-resolved analyses were then reduced off-line with in-house developed software written in R (Solari and Tanner, 2011), and the output was then imported into Excel, where the concordia as well as age-error calculations were obtained with Isoplot v. 3.70 (Ludwig, 2008).

During the analytical sessions in which the data presented in this paper were measured, the observed uncertainties (1sigma relative standard deviation) on the $^{206}Pb/^{238}U$, $^{207}Pb/^{206}Pb$ and $^{208}Pb/^{232}Th$ ratios measured on the Plešovice standard zircon were 0.75, 1.1 and 0.95 % respectively. These errors were quadratically added to the quoted uncertainties observed on the measured isotopic ratios of the unknown zircons. This last factor takes into account the heterogeneities of the natural standard zircons. Provided that the isotope ^{204}Pb, used to correct for initial common Pb, was not measured (because its tiny signal is swamped by the ^{204}Hg normally present in the He carrier gas), the common Pb was thus evaluated with the $^{207}Pb/^{206}Pb$ ratio, and all the analyses carefully graphed on Tera and Wasserburg (1972) diagrams. Correction, if needed, was then performed with the algebraic method of Andersen (2002). In figures, tables and results $^{206}Pb/^{238}U$ ages are used for zircons < 1.0 Ga, whereas $^{207}Pb/^{206}Pb$ ages are cited for older grains. The TuffZirc algorithm of Ludwig and Mundil (2002) was used to calculate the best mean of $^{206}Pb/^{238}U$ ages, which is preferred for estimating the apparent age of those young zircons in which the ^{207}Pb signal is low and thus yields imprecise results. The $^{207}Pb/^{206}Pb$ ages were furthermore considered as minimum ages because of the effect of possible Pb loss. We sampled granitic megaclasts in the Cañada de Tarachi Unit.

$^{40}Ar/^{39}Ar$ Method

A K-feldspar mineral separation from a selected rock sample was carried out by standard methods at the mineral separation laboratory at the Estación Regional del Noreste, Instituto de Geología, UNAM. Age analyses were carried out at Queen's University $^{40}Ar/^{39}Ar$ geochronology laboratory, Kingston, Canada. For each mineral separate, ~5–10 mg samples of material were wrapped in Al-foil and stacked vertically into Al canisters, which were then irradiated in the McMaster University Nuclear Reactor in Hamilton, Canada, with a $^{40}Ar/^{39}Ar$ flux monitor Hb3gr hornblende (1072 ± 11 Ma [2σ]; Roddick, 1983). Following irradiation, the samples and monitors were placed in small pits, ~2 mm in diameter, drilled in a Cu sample holder. The holders were placed inside a small, bakeable, stainless steel chamber with a Zn Se viewport connected to an ultra-high vacuum purification system. Monitors were fused in a single step; with a focused New Wave MIR-10 30 W CO_2 laser. For the step heating experiments, the laser beam was focused at different temperatures on mineral separates or whole rock samples in approximately 10 steps. The evolved gases were purified with an SAES C50 getter for ~5 min. Argon isotopes were measured with a MAP 216 mass spectrometer, with a Bäur Signer source and an electron multiplier. All data were corrected for blanks, atmospheric contamination, and neutron-induced interferences (Roddick, 1983; Onstott and Peacock, 1987). All errors are reported as ±2σ, unless otherwise noted, and dates were calculated using the decay constants recommended by Steiger and Jäger (1977).

Paleostress analysis

The stress inversion method was applied with Win_Tensor software (Delvaux, 1993). The inversion is based on the assumption that slip planes occur in the direction of the maximum resolved shear stress. The slip direction at a fault surface is inferred from the striations' slip-fiber lineations as a product of friction. Also, we determined the type of fault (normal or strike-slip) using drag folds that allowed us to discriminate faulting. Therefore, the strike and dip of the fault surfaces, the orientation of the lineation (pitch) and the sense of movement

identified at the fault surface were the data used for the inversion.

The obtained fault slip data were used to compute the four parameters of the reduced stress tensor according to Angelier (1994): the principal stress axes were S_1 (maximum compression), S_2 (intermediate compression) and S_3 (minimum compression), and the ratio of principal stress differences is $R = (S_2 - S_3) / (S_1 - S_3)$. The four parameters were determined by successive use of an improved version of the right dihedral method of Angelier and Mechler (1977) and a four-dimensional numeric rotational optimization using the Tensor computer program of Delvaux (1993).

Local Geology

In the study area two units of Upper Cretaceous age have been defined: 1) Cañada de Tarachi Unit, and 2) El Potrero Grande Unit and the Oligocene-Miocene Sierra Madre Occidental Cenozoic volcanic sequence (Figure 3).

Cañada de Tarachi Unit

The oldest unit, known as the Cañada de Tarachi, a name taken from the arroyo of the same name, is located south-east of Arivechi (Figure 3).The Cañada de Tarachi Unit consists of a sequence of conglomerate, sandstone, siltstone, shale, and interbedded

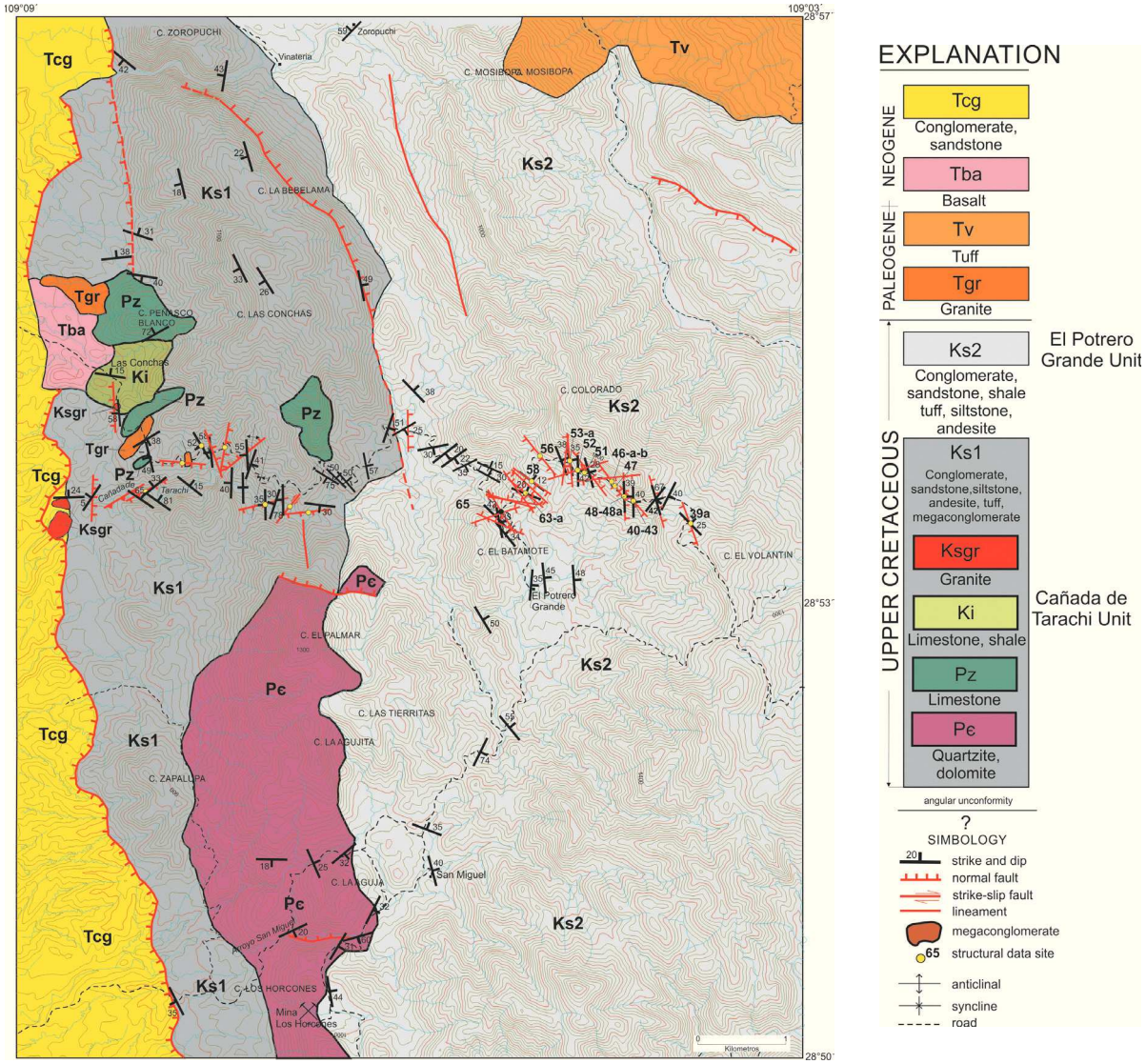

Figure 3. Geologic map of Cerro Las Conchas-Cerro El Volantín area, east of Arivechi, Sonora, Mexico.

andesitic tuffs, with a significant presence of monoliths (Blair and McPherson, 1999) comprised of Precambrian, Paleozoic and Mesozoic sedimentary and igneous rocks. The conglomerate beds in the sequence are composed of several lithologies located at different levels; some of them form a package over 100 m, but most are metric in thickness (Figure 4). The conglomerates originated as a debris flow. Some of the conglomerates in the lower level are of volcanic origin and rounded shape, well sorted, with clast size ranging between 2 and 10 cm, although a few of them measure 20 cm (Figure 4a and 4b); the conglomerates derived from sedimentary rocks are generally angular in shape and unsorted (Figure 4c and 4d).The whole Cañada de Tarachi Unit, on the other hand, records a strong deformation, which is believed to be synsedimentary and related to the gravitational movements of the megaclasts caused by vertical uplift and sliding, rather than the result of a compressive tectonic deformation.

The Precambrian monolith is exposed at Cerro El Palmar (Figure 5a), south of arroyo

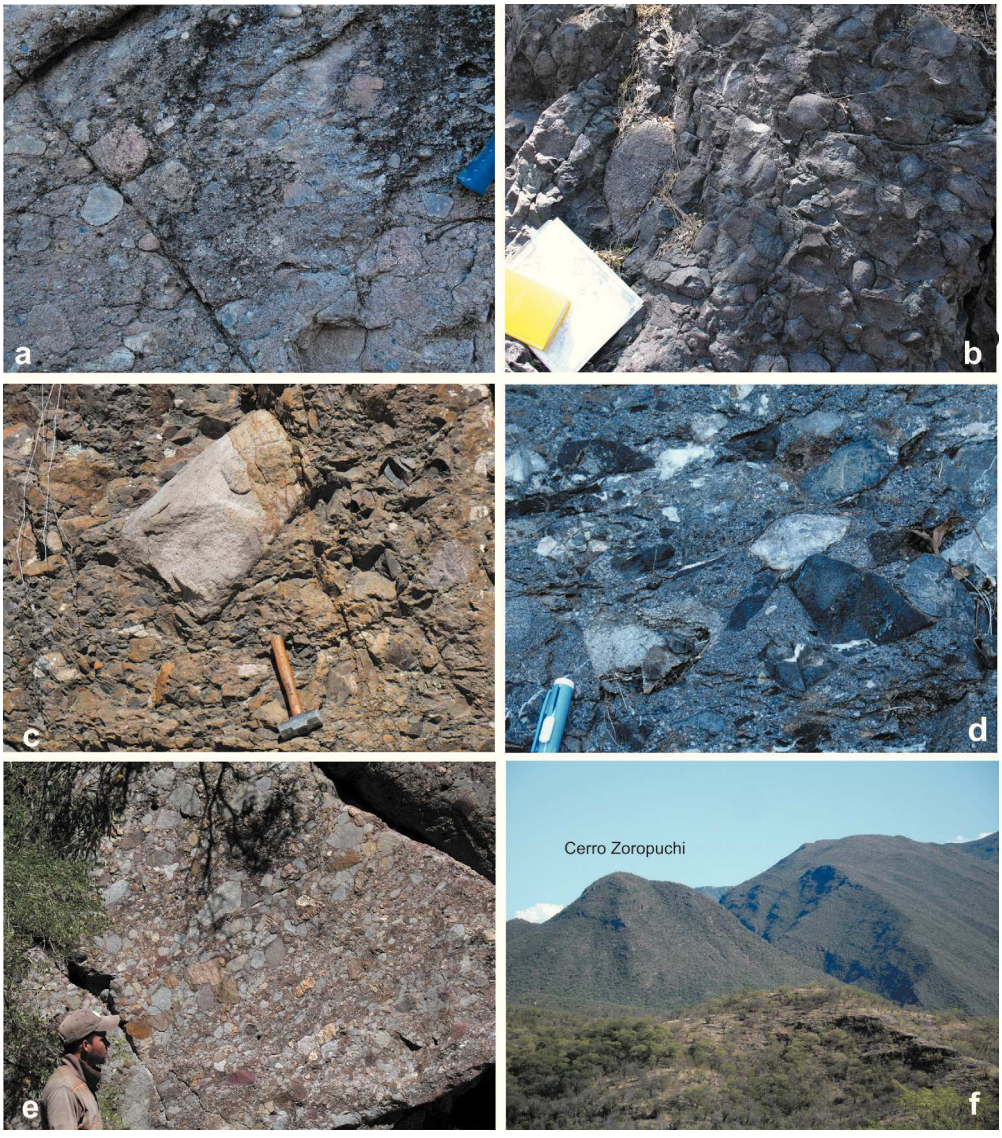

Figure 4. Conglomerate in Cañada de Tarachi Unit showing variation in composition and poor sorting. Images a and b show a conglomerate consisting of rock clasts derived from volcanic rocks which are more or less spherical in shape. Images c and d show a conglomerate consisting mainly of angular-shaped sedimentary clast rocks in a quartz-rich matrix. Images e and f show a conglomerate exposed to the north of the area in Cerro Zoropuchi (f) and in the range to the right. Here, the conglomerate is entirely composed of both Paleozoic and Lower Cretaceous limestone rock rounded clasts.

Cañada de Tarachi. The monolith consists of layers of quartz sandstone and dolomite. It measures 7 km long and 2 km wide. The contact between rocks of the Neoproterozoic and the Cañada de Tarachi Unit are marked by a breccia over 10 m thick.

At the base of the monolith, near the contact with the Upper Cretaceous rocks, along the arroyo San Miguel an important finding was the presence of stromatolite fossils, possibly of the *Jacutophyton* genus, similar to those found in the Caborca region (Weber *et al*., 1979) assigned to the Neoproterozoic. The monoliths of Paleozoic rocks (Figure 5b) are 2 km long, and consist of fossiliferous limestone and quartz sandstone which are assigned to the Mississippian by their fossil contents (Fernández-Aguirre and Almazán-Vazquez, 1991). These megablocks can be observed at Cerro Peñasco Blanco and Cerro Las Conchas.

At Cerro Las Conchas, another monolith composed of limestone, shale and sandstone and containing fossils from the Early Cretaceous (Fernández-Aguirre and Almazán-Vazquez, 1991) (Figure 3) is exposed. Bartolini (1993) suggested that these megaclasts have better correlation with exposed units in western Chihuahua than with rocks of the same age cropping out in Sonora.

We found several megaclasts composed of granite, and from these we selected two for dating. One was collected in the arroyo Cañada de Tarachi and was dated by U/Pb zircon geochronology at 76.00 ± 2 Ma (Campanian, Late Cretaceous, Figure 6a and 6b, Table 1), and a second sample around 100 m distant was collected at the Arivechi-Tarachi road and dated by $^{40}Ar/^{39}Ar$ step-heating of a k-spar at 69.57 ± 0.48 Ma (Figure 6c, Table 2). It was noted that these megaclasts are not only found on top but also within the sequence, in smaller thicknesses of dozens of meters. The fact that these are glided fragments, and because of their size were not previously identified as megaclasts, was the main reason for assuming that the stratigraphy was complicated and incorrectly interpreted by previous authors. Hence, we consider that the exposures of Cerro Las Conchas and the Paleozoic limestones are actually gliding megaclasts that are not "in situ."

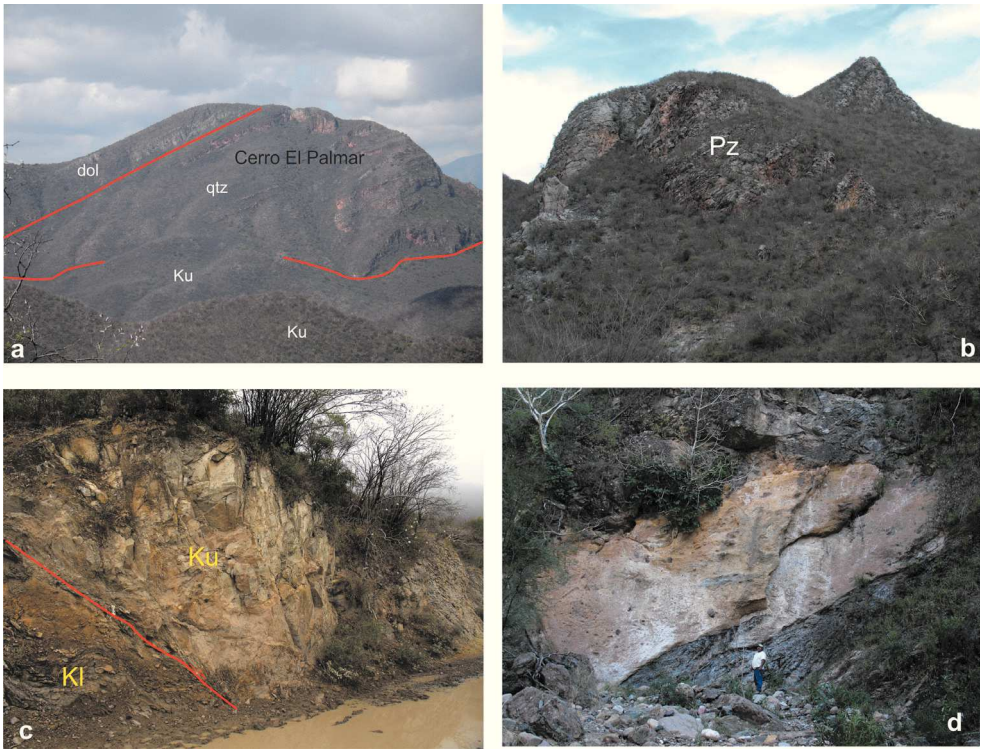

Figure 5. Megaclasts exposed in the Arivechi region. a) megaclast composed of quartzite and dolomite of Proterozoic age constituting Cerro El Palmar. In the forefront is the conglomerate that, together with the megablock, forms part of the Cañada de Tarachi Unit. dol = dolomite, qtz = quartzite, Ku = volcano-sedimentary rocks. b) Paleozoic limestone megaclast. North view. c) 76 Ma granite block (Ku) which is jammed in Lower Cretaceous rocks (Kl). Note the deformation in the rocks of the Lower Cretaceous (Ki). d) Megaclast of uncertain age embedded in the Cañada de Tarachi Unit. Outcrop along the arroyo Cañada de Tarachi.

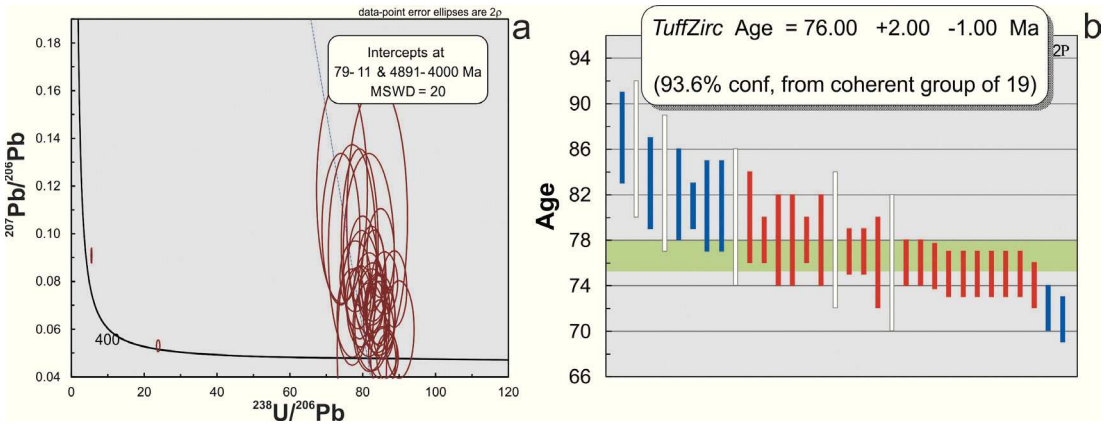

Figure 6. U/Pb zircon data from the granite megablock in the Cañada de Tarachi. a) Concordia curve for the A134-12 sample and b) Weighted mean age graph at 76 Ma.c) Ar/Ar data from the Arivechi-Tarachi road.

Table 1. U-Pb analytical data for zircons from sample in eastern Sonora, Arivechi region.

				CORRECTED RATIOS									CORRECTED AGES (Ma)							
	U (ppm)	Th (ppm)	Th/U	207Pb/206P	±1s	207Pb/235I	±1s	206Pb/238I	±1s	208Pb/232T	±1s	Rho	206Pb/238	±1s	207Pb/235	±1s	207Pb/206P	±1s	Best age (Ma)	±1s
Zircon_01_A134_0	132	89	0.62	0.07556	0.00499	0.12377	0.0085	0.01209	0.00022	0.00398	0.0002	0.26	77	1	118	8	1083	120	77	1
Zircon_02_009	89	41	0.42	0.04985	0.02102	0.08613	0.0405	0.01253	0.00044	0.00396	0.0012	0.22	80	3	84	38	188	607	80	3
Zircon_04_011	169	164	0.89	0.06256	0.00394	0.1	0.0064	0.01181	0.00015	0.00388	0.00017	0.2	75.7	1	97	6	693	121	76	1
Zircon_05_012	77	54	0.65	0.10648	0.023	0.17487	0.0427	0.01191	0.00048	0.00346	0.00013	0.37	76	3	164	37	1740	375	76	3
Zircon_06_014	84	55	0.60	0.08532	0.00725	0.13924	0.0121	0.01213	0.00022	0.00387	0.0003	0.21	78	1	132	11	1323	149	78	1
Zircon_07_015	183	119	0.60	0.05961	0.00501	0.09596	0.0082	0.01167	0.00016	0.00381	0.00016	0.16	75	1	93	8	589	165	75	1
Zircon_08_016	88	46	0.48	0.06502	0.00823	0.11625	0.0156	0.01297	0.00028	0.00397	0.00009	0.19	83	2	112	14	775	243	83	2
Zircon_09_017	54	24	0.41	0.10192	0.01297	0.18986	0.0262	0.01351	0.00039	0.00394	0.00011	0.26	87	2	177	22	1659	216	87	2
Zircon_10_018	69	44	0.58	0.09574	0.01627	0.15783	0.0271	0.01263	0.00033	0.00391	0.00031	0.15	81	2	149	24	1543	300	81	2
Zircon_11_020	145	81	0.51	0.06455	0.00631	0.10525	0.0112	0.01182	0.00025	0.00362	0.00008	0.23	76	2	102	10	760	187	76	2
Zircon_12_021	115	74	0.59	0.06171	0.00784	0.10303	0.014	0.01211	0.00029	0.00373	0.00009	0.21	78	2	100	13	664	248	78	2
Zircon_13_022	170	105	0.57	0.04817	0.00409	0.07621	0.0066	0.01152	0.00016	0.00324	0.00017	0.17	74	1	75	6	108	164	74	1
Zircon_14_023	747	153	0.19	0.05302	0.00101	0.30621	0.0063	0.04194	0.00033	0.01285	0.00035	0.38	265	2	271	5	330	39	265	2
Zircon_15_024	162	101	0.57	0.05985	0.00834	0.0917	0.0136	0.01111	0.00021	0.00343	0.00009	0.22	71	1	89	13	598	270	71	1
Zircon_16_026	107	62	0.53	0.09189	0.00761	0.14917	0.0134	0.01177	0.00021	0.00347	0.00006	0.26	75	1	141	12	1465	142	75	1
Zircon_17_027	113	68	0.55	0.0681	0.00586	0.11014	0.0096	0.01189	0.00019	0.00345	0.00022	0.18	76	1	106	9	872	162	76	1
Zircon_18_028	291	305	0.96	0.06083	0.00759	0.10248	0.0142	0.01222	0.00027	0.00377	0.00007	0.32	78	2	99	13	633	245	78	2
Zircon_19_029	174	121	0.64	0.04999	0.00451	0.0806	0.008	0.01169	0.00022	0.00369	0.0001	0.23	75	1	79	8	195	177	75	1
Zircon_20_030	173	142	0.75	0.07936	0.00532	0.12459	0.0086	0.01163	0.0002	0.0034	0.00014	0.24	75	1	119	8	1181	120	75	1
Zircon_22_033	144	95	0.61	0.06527	0.00718	0.10488	0.0117	0.01177	0.00022	0.00376	0.00022	0.17	75	1	101	11	783	210	75	1
Zircon_23_034	122	98	0.74	0.08817	0.00785	0.15383	0.014	0.0125	0.00025	0.00409	0.00026	0.22	80	2	145	12	1386	155	80	2
Zircon_24_035	134	126	0.86	0.11804	0.01929	0.21902	0.0411	0.01346	0.00052	0.00386	0.00015	0.49	86	3	201	34	1927	273	86	3
Zircon_25_036	167	120	0.66	0.07309	0.00526	0.12506	0.0093	0.0127	0.00023	0.00384	0.00021	0.24	81	1	120	8	1016	132	81	1
Zircon_26_038	124	81	0.59	0.06843	0.00602	0.10815	0.0097	0.01191	0.0002	0.00366	0.00018	0.19	76	1	104	9	882	165	76	1
Zircon_27_039	150	119	0.73	0.04727	0.00538	0.0761	0.0092	0.01168	0.00019	0.00371	0.00021	0.23	75	1	74	9	63	242	75	1
Zircon_28_040	115	140	1.12	0.08211	0.00608	0.14711	0.0114	0.01283	0.00028	0.00426	0.00033	0.28	82	2	139	10	1248	149	82	2
Zircon_29_041	49	29	0.54	0.09109	0.01738	0.15376	0.0311	0.01224	0.00043	0.00361	0.00014	0.27	78	3	145	27	1448	399	78	3
Zircon_30_042	108	63	0.54	0.06953	0.00695	0.11963	0.0122	0.01258	0.00025	0.00338	0.00023	0.2	81	2	115	11	915	214	81	2
Zircon_31_044	114	71	0.57	0.07682	0.00653	0.11577	0.01	0.01128	0.00018	0.00302	0.00023	0.18	72	1	111	9	1117	175	72	1
Zircon_32_045	131	80	0.56	0.07508	0.00691	0.12143	0.0115	0.01223	0.00026	0.00405	0.00019	0.22	78	2	116	10	1071	191	78	2
Zircon_33_046	134	91	0.62	0.07349	0.00478	0.12048	0.0081	0.01211	0.00022	0.00386	0.00017	0.27	78	1	116	7	1027	135	78	1
Zircon_34_047	56	35	0.57	0.09276	0.0182	0.16579	0.0352	0.01296	0.00045	0.00382	0.00014	0.29	83	3	156	31	1483	410	83	3
Zircon_35_048	126	59	0.43	0.07996	0.0088	0.12791	0.0142	0.01204	0.0002	0.0042	0.00031	0.15	77	1	122	13	1196	227	77	1
Zircon_03_010	784	181	0.21	0.09084	0.00127	2.2649	0.0369	0.18068	0.0015	0.04054	0.00264	0.51	1071	8	1201	11	1443	27	1443	27

Table 2. $^{40}Ar/^{39}Ar$ analytical data from sample in eastern Sonora, Arivechi region.

Sample no	Mineral		J	± (1s)	% error		Int Age (Ma)	± (2 s)	with ± in J		Plateau Age	± (2s)	with ± in J	MSWD	% 39Ar	Probability	Initial Ratio	Initial Ratio Error	
JR13	KSP		0.003655	0.000006	0.16		68.84	0.52	0.57		69.51	0.49	0.54	1.20	87.76				
Can/Pos	221/JR13	AOR13-13								IsoPlot PA-->	69.57	0.48	na	1.30	78.7	0.24	na	na	
						Decay corrected true ratios				IsoPlot CA-->	70.07	0.65	na	1.70	100.00	0.06	284.30	6.60	
Step no	Power	40Ar/39Ar	±	38Ar/39Ar	±	37Ar/39Ar	±	36Ar/39Ar	±	40Ar*/39Ar(K)	±	40Ar*	Cumulative 39Ar (%)	Age	±	Ca/K	±	Cl/K	±
	(%)		(1 s)		(1 s)		(1 s)		(1 s)		(1 s)	(%)		(Ma)	(1 s)		(1 s)		(1 s)
1	2.5	67.695	0.577	0.221	0.006	0.133	0.211	0.203	0.004	7.803	1.137	11.5	1.23	50.73	7.29	0.24	0.39	0.0390	0.00
2	3.0	39.928	0.269	0.127	0.003	0.353	0.126	0.101	0.002	10.115	0.595	25.3	3.14	65.49	3.78	0.65	0.23	0.0217	0.00
3	3.5	24.151	0.150	0.068	0.002	0.482	0.097	0.049	0.001	9.801	0.359	40.6	6.24	63.50	2.28	0.88	0.18	0.0104	0.00
4	4.0	17.554	0.074	0.043	0.001	0.998	0.053	0.025	0.001	10.288	0.185	58.6	12.23	66.60	1.17	1.83	0.13	0.0056	0.00
5	4.5	15.658	0.065	0.032	0.001	1.302	0.060	0.017	0.001	10.685	0.179	68.2	18.19	69.11	1.13	2.39	0.16	0.0034	0.00
6	5.5	15.091	0.042	0.027	0.001	2.350	0.047	0.015	0.000	10.841	0.100	71.7	30.58	70.10	0.64	4.31	0.22	0.0023	0.00
7	6.5	13.992	0.042	0.023	0.001	2.189	0.044	0.011	0.000	10.860	0.098	77.5	41.85	70.22	0.62	4.01	0.20	0.0015	0.00
8	7.5	13.156	0.039	0.020	0.001	1.952	0.047	0.008	0.000	10.832	0.106	82.2	52.13	70.05	0.67	3.58	0.19	0.0011	0.00
9	8.5	12.381	0.044	0.018	0.001	1.581	0.049	0.006	0.000	10.859	0.097	87.6	61.81	70.22	0.62	2.90	0.16	0.0008	0.00
10	10.0	12.143	0.045	0.022	0.001	0.995	0.040	0.005	0.000	10.624	0.099	87.4	70.32	68.73	0.63	1.82	0.11	0.0016	0.00
11	12.0	12.122	0.054	0.033	0.001	0.690	0.042	0.005	0.000	10.669	0.115	88.0	77.72	69.01	0.73	1.26	0.10	0.0042	0.00
12	15.0	12.299	0.078	0.051	0.001	0.522	0.053	0.006	0.000	10.484	0.153	85.2	83.26	67.84	0.97	0.95	0.11	0.0083	0.00
13	18.0	12.902	0.079	0.066	0.001	0.513	0.095	0.008	0.001	10.548	0.185	81.7	87.88	68.25	1.17	0.94	0.18	0.0117	0.00
14	22.0	14.154	0.099	0.103	0.002	0.664	0.099	0.011	0.001	11.037	0.275	77.9	90.94	71.35	1.74	1.22	0.19	0.0200	0.00
15	30.0	15.351	0.093	0.145	0.002	0.733	0.038	0.016	0.000	10.645	0.149	69.3	100.00	68.86	0.95	1.34	0.09	0.0293	0.00

No fossils have been identified in the Cañada de Tarachi Unit, apart from those that are contained in the slipped blocks. This statement has genetic significance for the sedimentary environment. The absence of fossils could be interpreted as resulting from the development of these basins inland. In terms of the thickness of this unit, based on the conducted mapping and strike and slip directions, we estimated that it must have a minimum thickness of 2000 m.

Fossil studies carried out on the conglomerate clasts indicate Paleozoic and Early Cretaceous ages; therefore the Cañada de Tarachi Unit is situated in the Upper Cretaceous sequence. The 76 Ma U/Pb zircon date for the granite block at the Cañada de Tarachi Unit was interpreted as the crystallization date and the 70 Ma $^{40}Ar/^{39}Ar$ date was interpreted as the cooling age, i.e., postdating a Late Cretaceous age and suggesting that the onset of erosion was probably present by that time.

The base of the Cañada de Tarachi Unit is not exposed, but from correlation with other localities it has been interpreted as an angular unconformity unit over older rocks; in addition, the upper contact with the El Potrero Grande Unit is transitional to a younger volcaniclastic sequence.

El Potrero Grande Unit

This unit takes its name from the ranch located south-east of Cerro El Batamote (Figure 3). King (1939) defines this as the Potrero Formation, which seems to correspond to the same location, although he assigns it to the Albian. The El Potrero Grande Unit is much more of a volcano-sedimentary sequence than the Cañada de Tarachi Unit. The El Potrero Grande Unit consists of conglomerate, sandstone, siltstone, and shale with interbedded andesite, diorite strata dikes and layers of rhyolitic tuffs. These rocks together form a partial column more than 2,400 m thick (Figure 7). It must be said that we did not measure the entire El Potrero Grande Unit, because it is covered by Tertiary volcanic to the east.

The base of the unit consists of a section of conglomerates and volcanic rocks of andesitic composition that includes tuffs, continuing with shale, siltstone and sandstone that form a rhythmic sequence.

Isotopic K/Ar ages in biotite concentrates from volcanic rocks provided dates of 83.4 ± 4.17Ma (Pubellier, 1987), 84 and 86 Ma K-Ar, respectively, for two tuffs in the upper part of the sequence, indicating an Upper Cretaceous age for the sequence (Grajales-Nishimura *et al*., 1990). In the Sahuaripa-Natora road we dated a tuff in a similar section 20 km north of the area. The age sample was dated as 76.3 ± 1.98 Ma (U/Pb zircon at Geociencias isotopic Lab), placing it in the Campanian (Upper Cretaceous). We consider this tuff equivalent in age to tuffs in our study area.

The Upper Cretaceous in Arivechi, eastern Sonora was deposited in a deep sedimentary basin that received sediments from an existing volcanic arc and also accumulated sediments from both the exposed north-western and north-eastern basement.

Structural Geology

The structures found in the study area are normal and strike-slip faults, as well as mesoscopic folds. They are the result of two different processes recorded in the Upper Cretaceous units. The older mechanism is a Cretaceous gravitational gliding deformation, which affects only the Cañada de Tarachi Unit; the El Potrero Unit shows only extension and the associated structures.

Gliding tectonics is interpreted as a mechanism whereby large masses of rocks move down a slope under gravitational force, producing folding and faulting at different extents and complexity. The fine-grained rocks of the Cañada de Tarachi Unit are folded into smaller tight folds as seen along the arroyo Cañada de Tarachi. The structures are–considered synsedimentary in order to denote their inferred formational environment, and include extensional faulting and reverse faults and folds.

In northern Sonora, Rodriguez-Castañeda (2002) interpreted a similar sequence formed by gravitational re-sedimentation generated by tectonic activity along the south-west margin of the Cananea High, a positive land that could be the continuation of the Aldama Platform into Sonora.

The extensional faults are observed along the two units whereas contractional structures are restricted to the thin bedded sandstone and siltstone exposed in the front of the sliding mass observed in the Cañada de Tarachi Unit.

Fold data collected from the Cañada de Tarachi Unit indicate that folds are asymmetric and related to detachment surfaces. The fold vergence (Figure 8) suggests that the sequence was transported towards the south-west and to a lesser extent towards the north-east. Figure 9 corresponds to "Z" fold kinematic indicators,

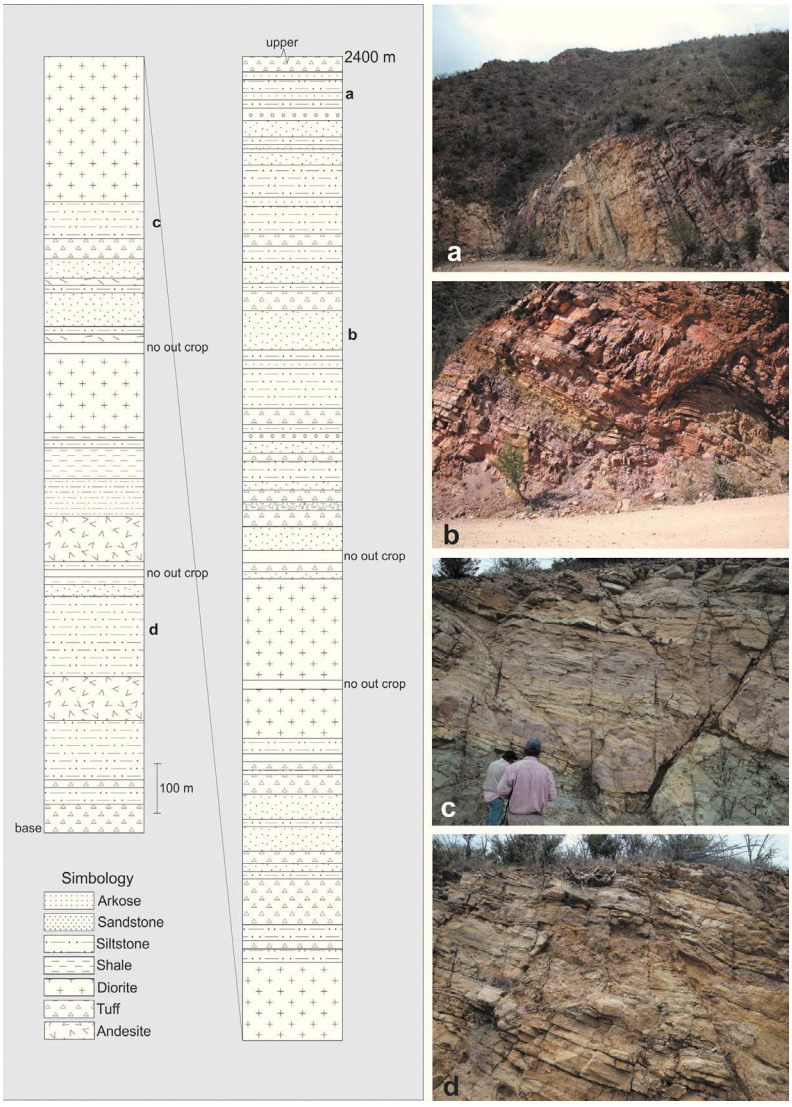

Figure 7. A 2,400 m measured column on a segment of the El Potrero Grande Unit, from the Cerro El Volantín to the Cerro El Batamote. Pictures go from top to bottom, i.e., from **a** to **d**. The **bold** letters in the lithologic column show the approximate location of the picture in the column. Compare the structures observed in the El Potrero Grande Unit with structures recorded in the Cañada de Tarachi Unit in Figure 9.

showing vergence towards the south-west. In Figure 9a the layer that serves as detachment for the formation of folds has a 019 strike with a 30NW dip. Most of the folds display axial surfaces oriented NW-SE and plunging to the north-east with two *arrays*, one with an average of 83° and the second with an average of 34°.

The folds show no obvious genetic relationship to tectonic contraction within the megaclasts. It is clear that folds are related to a synsedimentary deformation corresponding to the emplacement of the megaclast as indicated by its geometry and location.

Normal faulting and paleostress reconstruction

To explain the tectonic processes from which the development of these structures originated, a paleostress field reconstruction is offered. The paleostress analysis was performed with measured surface data collected over faults in the Upper Cretaceous rocks along the Arivechi-Tarachi road, in the section between Cerro Las Conchas and Cerro El Volantín and along the arroyo Cañada de Tarachi. The data sites are located in sedimentary rocks as much as in igneous rocks. The displacement over the measured faults is generally from centimeters up to meters, and the faults are normal, although some of them record a strike-slip component. In general, all the measured faults display good striations. The results obtained from the paleostress analysis are in shown in Table 3 and in Figures 10 and 11.

The evolution of the stress fields is shown in structural maps (Figures 12 and 13) with symbols indicating the two horizontal S_{Hmax} and

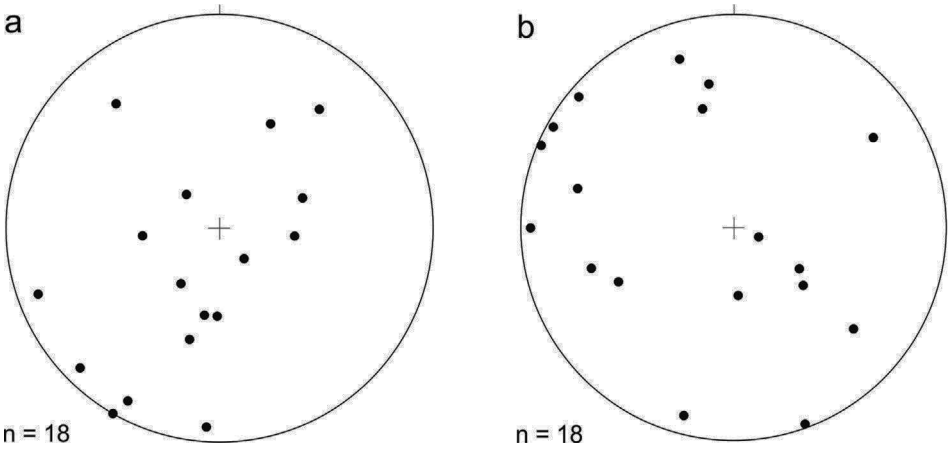

Figure 8. Folds in Cañada de Tarachi Unit. a) Poles of axial surfaces showing south-west vergence. b) Fold hinge lines showing a horizontal to sub-vertical plunge oriented NW-SE.

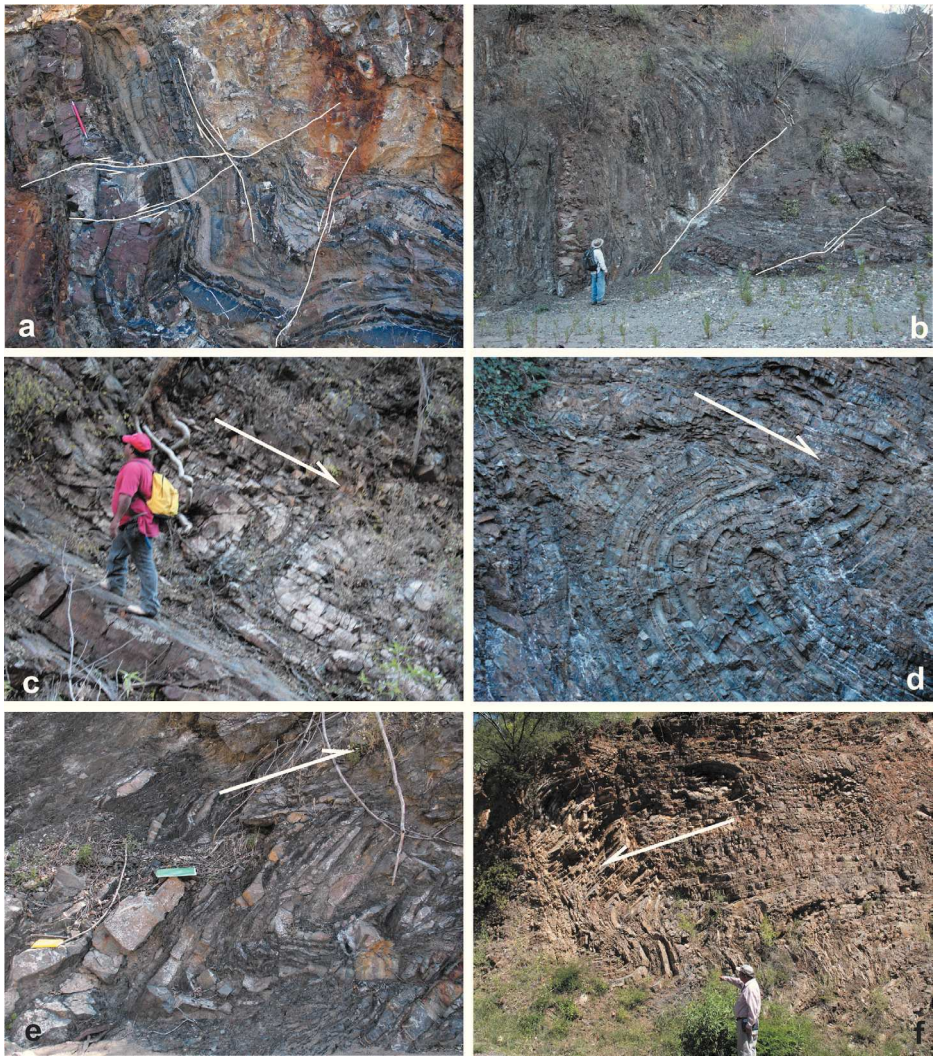

Figure 9. Intense deformation (a and b) recorded in the base of the Cañada de Tarachi Unit. Note the scale of deformation. Reverse and normal faults plus folds affect the sequence. Z folds recorded in the Cañada de Tarachi Unit (c, e, d) suggest transport to the south-west. In a, the bed where the man stand is the base of the detachment. The S fold on f crops out along the Arivechi-Tarachi road, also suggesting transport to the west.

S_{hmin}, with black inward arrows for compressive stress and white outward arrows for extensive stress. The length depends on the magnitude of the relative stress in function of the stress relation *R* and orientation of the principal stress directions. The vertical axis is indicated by an open circle for a compressive regime (vertical extension), by a dot for a strike-slip regime, and by a black circle for an extensive regime (vertical compression). The classifications proposed by Delvaux *et al*. (1995) for the stress tensors are: *radial / pure / strike-slip* extensive, *extensive / pure / compressive* strike-slip or *strike slip / pure / radial* compressive based on the relative magnitude of the intermediate axis and given by the stress relation *R* (Figure 14).

The orientation of the stress field was determined with the measured structures which show a clear sense of movement. Twenty-six sites were examined in the studied sector. The sites are located in outcrops of Upper Cretaceous rocks. The results of the inversion (Table 3) and their correlation allow the definition of several paleostress groups. The tensors are grouped according to their similarity, based on the direction of the main axes S_{Hmax}, $S_{hmi,}$ the stress regime index and the stratigraphic relation.

The faulted sediments, which belong to the Cañada de Tarachi Unit, dip towards the north-east. Almost all the faults are normal

Table 3. Parameters of the paleostress tensors calculated for rocks of the Upper Cretaceous.

Site	Lithology	n	S1	S2	S3	R	R´	Type of tensor
Data of Cañada de Tarachi Unit, ductile and fragile conditions								
A57-10	Conglomerate	8	109/45	317/42	214/14	0.44	0.44	Pure extensive
A57-10a	Conglomerate	8	019/24	184/65	288/06	0.44	1.56	Pure strike-slip
A71-10	Sandstone	7	260/58	099/31	004/08	0.42	0.42	Pure extensive
A72-10	Conglomerate	8	253/34	099/54	350/14	0.5	1.5	Pure strike-slip
A88-11	Sandstone	5	082/54	196/16	295/28	0.5	0.5	Pure extensive
A95-11	Sandstone	6	108/71	250/15	341/04	0.5	0.5	Pure extensive
A97-11	Sandstone	11	274/70	177/02	086/20	0.5	0.5	Pure extensive
Data El Potrero Grande Unit, fragile conditions								
A140-12	Sandstone	5	034/48	188/39	288/12	0.5	0.5	Pure extensive
A40-10	Tuff	6	098/39	257/00	360/11	0.5	1.5	Pure strike-slip
A41-10	Andesite	4	096/11	243/77	005/07	0.5	1.5	Pure strike-slip
A42-10	Andesite	8	325/38	107/46	220/20	0.5	0.5	Pure extensive
A43-10	Sandstone	7	333/42	111/39	221/22	0.5	0.5	Pure extensive
A46-10	Tuff	10	199/36	070/37	315/29	0.33	0.33	Pure extensive
A46-10a	Tuff	4	009/35	179/54	278/06	0.25	1.75	Compressive strike-slip
A46-10b	Tuff	8	067/68	329/03	238/23	0.38	0.38	Pure extensive
A47-10	Andesite	5	045/62	139/02	230/26	0.5	0.5	Pure extensive
A48-10	Andesite	14	100/44	256/43	359/14	0.5	0.5	Pure extensive
A48-10a	Andesite	4	097/35	248/51	356/14	0.5	1.5	Pure strike-slip
A51-10	Tuff	5	128/02	321/88	216/01	0.5	1.5	Pure strike-slip
A52-10	Tuff	6	161/77	069/00	339/08	0.88	1.12	Extensive strike-slip
A53-10	Sandstone	4	006/83	134/04	224/01	0.62	0.62	Pure extensive
A53-10a	Sandstone	5	090/64	347/07	253/28	0.5	0.5	Pure extensive
A56-10	Sandstone	5	113/35	274/53	016/09	0.7	1.3	Extensive strike-slip
A63-10	Tuff	5	174/80	306/07	036/06	0.4	0.4	Near pure extensive
A63-10a	Sandstone	5	051/66	163/09	256/14	0.5	0.5	Pure extensive
A65-10	Sandstone	4	324/29	147/61	054/01	0.5	1.5	Pure strike-slip

n= number of fault data used for stress tensor determination; s1, s2, s3 = plunge and azimuth of principal stress axes; R = stress ratio (s2 – s3)/(s1 – s3), R´ = tensor type index.

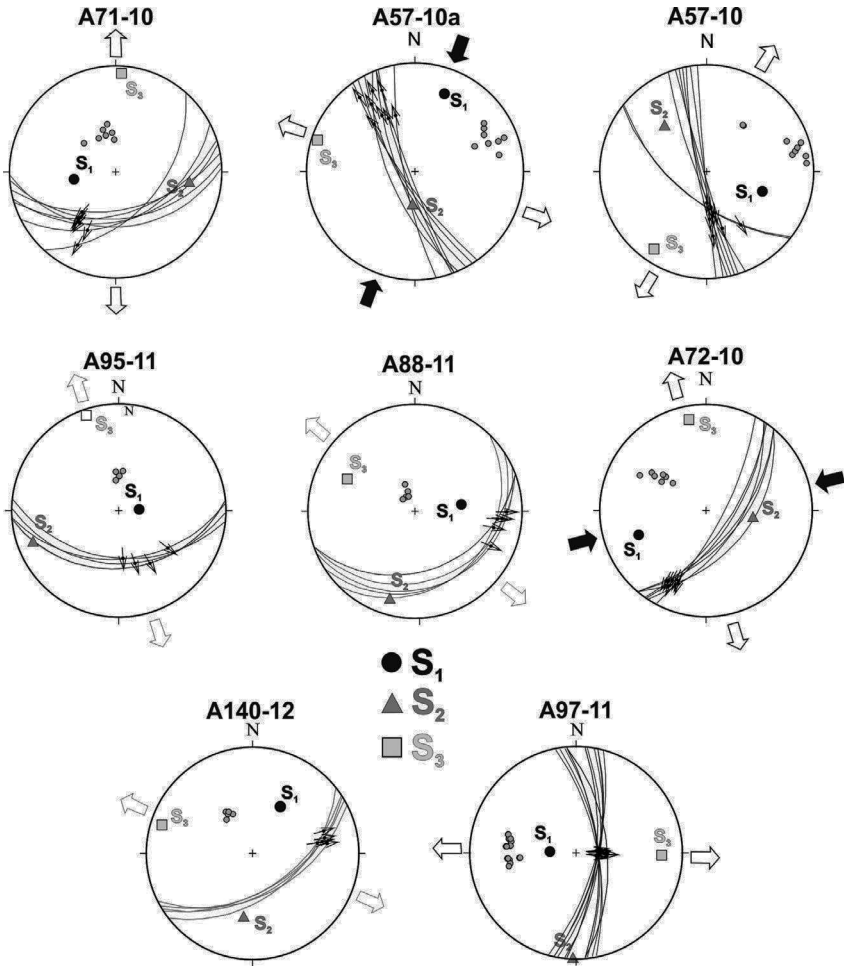

Figure 10. Paleostress reconstructions for the rocks of the Cañada de Tarachi Unit. Circle = S_1; Triangle = S_2; Square = S_3.

with oblique-slip motions predominating, but dip-slip and strike-slip are present and play an important role. Faults in Figure 13 show that the motion of these faults was induced by extension along a direction of S_3 NW-SE, NE-SW and E-W for dip-slip normal faults; whereas S_1 is in general NNE-WSW and ENE-WSW in relation to strike-slip faults (Figure 10).

On the other hand, at the El Potrero Grande Unit faults are dip-slip, oblique slip normal faults and strike-slip faults. The direction of S_3 is NE-SW for dip-slip normal faults; NE-SW, almost N-S, and NW-SE for the oblique normal faults, and the S_1 directions E-W, NW-SE, and WNW-ESW are related to strike-slip faults (Figure 11).

Evolution

The studies carried out in the area indicated the existence of two Cretaceous sequences differentiated by their composition and stratigraphic position. The observed structures are mesoscopic folds in the Cañada de Tarachi Unit and the development of normal faults and smaller proportion by strike-slip faults.

The Cañada de Tarachi Unit is characterized by intercalations of conglomerate, sandstone, siltstone, rhyolitic tuff and andesite, showing a strong deformation. The geographic extension of Precambrian, Paleozoic and Lower Cretaceous monoliths or remnant rocks suggests that they belong to a basement possibly located towards the east, in the State of Chihuahua. The fold vergence (Figure 8) indicates that the sequence was transported towards the south-west.

The directions of stress that we were able to determine from the Cañada de Tarachi Unit from normal oblique, normal dip-slip and strike-slip faulting are shown in Figures 10 and 12. Local results are given in Figure 12 for both minimum horizontal stress (S_3) and maximum stress (S_1). Extension stress (S_3) is more common than compression stress (S_1), because the normal faults (subverticalS_1) in the section are common whereas strike-slip faults moved when both compression and extension were horizontal (subverticalS_2). Normal faults with different orientations, such as NNW-SSE, NE-SW, E-W, and N-S, show high and medium dips (Figure 10). The

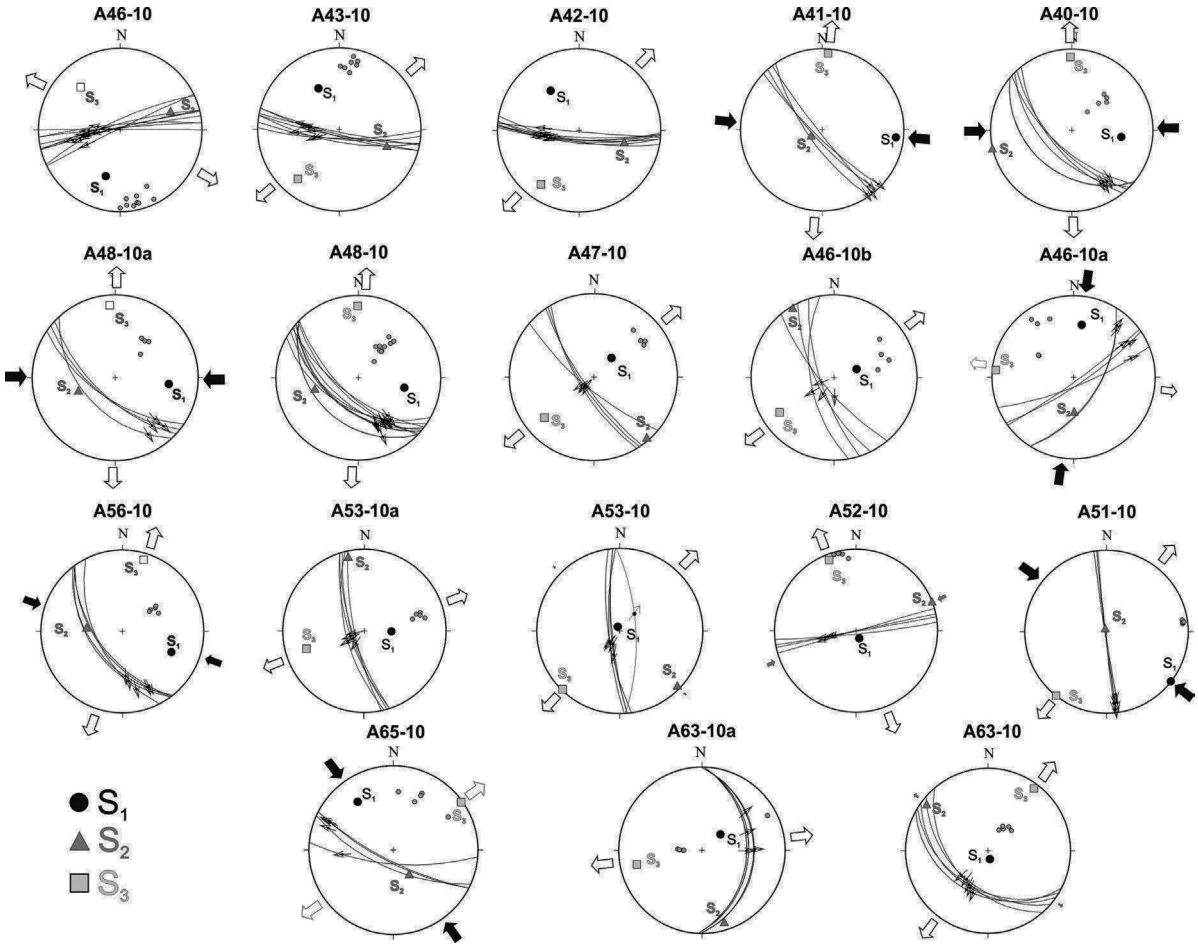

Figure 11. Paleostress reconstructions in the El Potrero Grande Unit. Circle = S_1, triangle = S_2, square = S_3.

faults with an oblique component in the NNW direction have high dips towards the west and were induced by the S_3 extension direction NE-SW; NE oblique faults have medium angle dips towards the south-east and are the result of a N-S and NW-SW S_3; E-W dip-normal faults dip towards the south with intermediate angles, whereas the N-S faults display high angle dips towards the east as a result of NNW S_3 and E-W S_3 directions, respectively (Figure 10). The strike-slip faults with NE-SW and NW-SE orientations characteristically have high angle dips associated with ENE-WSW and NNE-SSW compression (S_1), respectively (Figure 10).

The paleostress tensors are shown in Table 3 and in the structural planes of Figures 12 and 13. The tensors were grouped according to their similarities based on the stress regime and the direction of the stress axis. The paleostress is only recorded in Upper Cretaceous rocks, the reason why chronological ordering of paleostress data depends upon rock comparison with other sites outside the study area.

The Cañada de Tarachi Unit is characterized by an extension regime and, to a lesser degree, by a pure strike-slip regime (Figure 13). The main axis of extension (S_3) is almost horizontal with a NW-SE main direction, and with a smaller proportion in a NE-SW direction. The main axis of compression, corresponding to the strike-slip movements,(S_1) is sub-vertical with a NE-SW direction. In conclusion, the previous analysis shows that at the time there was an extension regime with development of high angle normal faults.

Interpretation of the paleostress results in the El Potrero Grande Unit indicates a stress regime characterized by extension and strike-slip regimes, both well defined (Figure 13). The extension regime displays an S_3 closer to the horizontal in a NE-SW direction (Figure 13). The strike-slip regime is shown by a varying

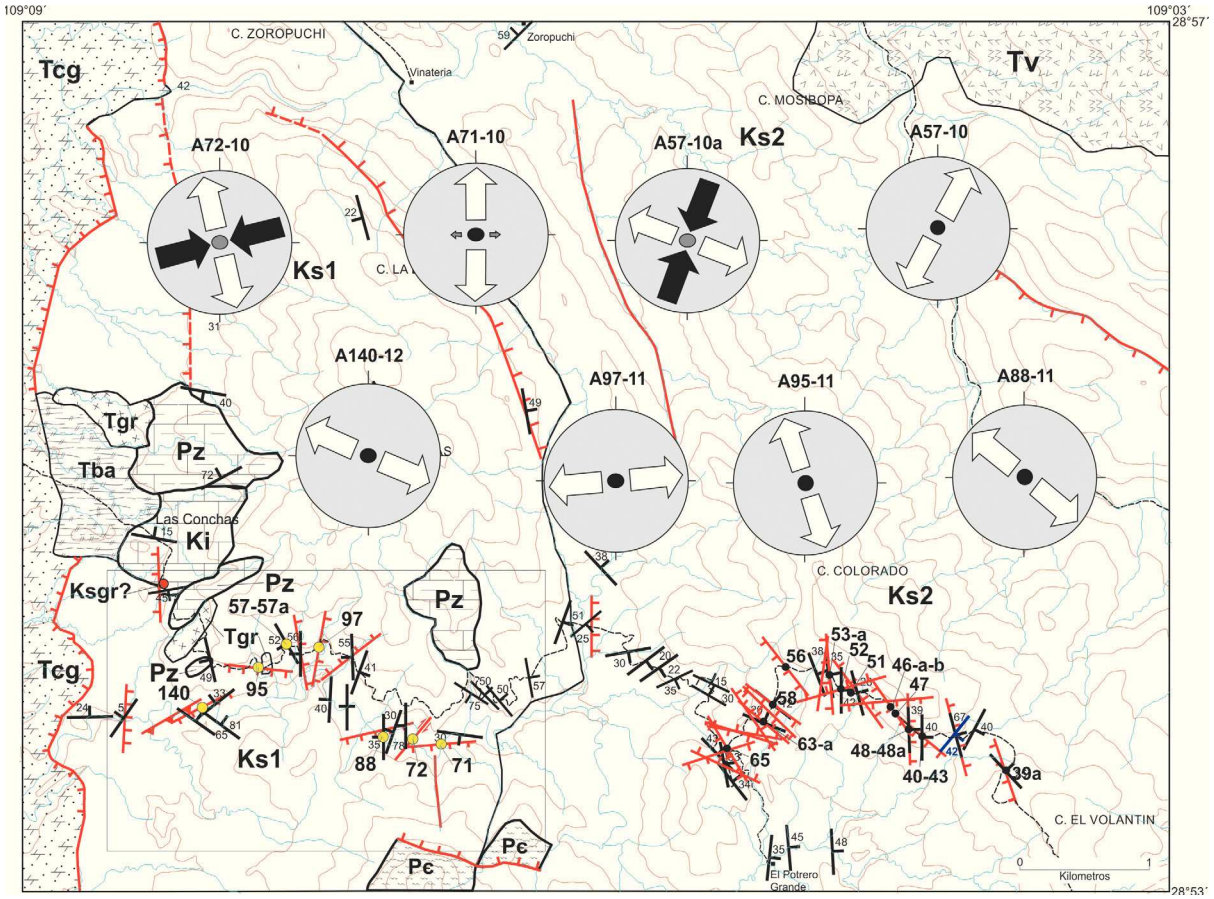

Figure 12.Orientation of the horizontal maximum and minimum stress in the Cañada de Tarachi Unit. The square shows the location of measured sites. Black arrow = S_1, white arrow = S_3. The central circle corresponds to S_1 when black and S_2 when gray.

main axis of compression S_1, almost horizontal in sites A41-10 and A51-10, sub-vertical in sites A40-10, A46-10a, A41-10, A48-10a, A56-10 and A65-10, and with almost E-W, NW-SE and N-S directions in site A46-10a. The stress of extension S_3 is horizontal to a N-S, NE-SW direction (Figure 13).

Discussions

The megaclasts identified in the study area range in age from the Proterozoic to the Mesozoic. Two megaclasts of granitic composition were dated, one by U/Pb date on zircon and one by $^{40}Ar/^{39}Ar$ step-heating date on K-spar, since they were less than 100 m apart, we assume that they were from the same pluton and therefore we can interpret the dates as concordant. One is an emplacement aged 76.0 ± 2.0 Ma by U/Pb zircon geochronology, and the second one gives a K-spar cooling age of 69.57 ± 0.48 Ma according to $^{40}Ar/^{39}Ar$ step-heating geochronology. It is assumed that the megaclasts are part of the same pluton and were deposited at the same time as part of a debris flow in an alluvial slope. The ages of the granitic blocks suggest that the minimum age for the onset of the erosion is not earlier than 76 Ma according to the U/Pb date. The difference in zircon U/Pb and K-feldspars $^{40}Ar/^{39}Ar$ concordant dates (76 Ma and 70 Ma, respectively) suggest rapid uplift and erosion. As a consequence of these processes, rapid uplift and erosion, the column of Cretaceous sediments is more than 10 km thick. The absence of fossils and the rhytmitic sedimentation at the youngest unit suggests a neritic or a lacustrine continental environment.

From a tectonic perspective, it can be considered that the recognized megaclasts were formed in an extensional environment where topographic highs were formed, causing block gliding. Our hypothesis is that the Arivechi area was located near or at the edge of the Aldama Platform. It is probable that

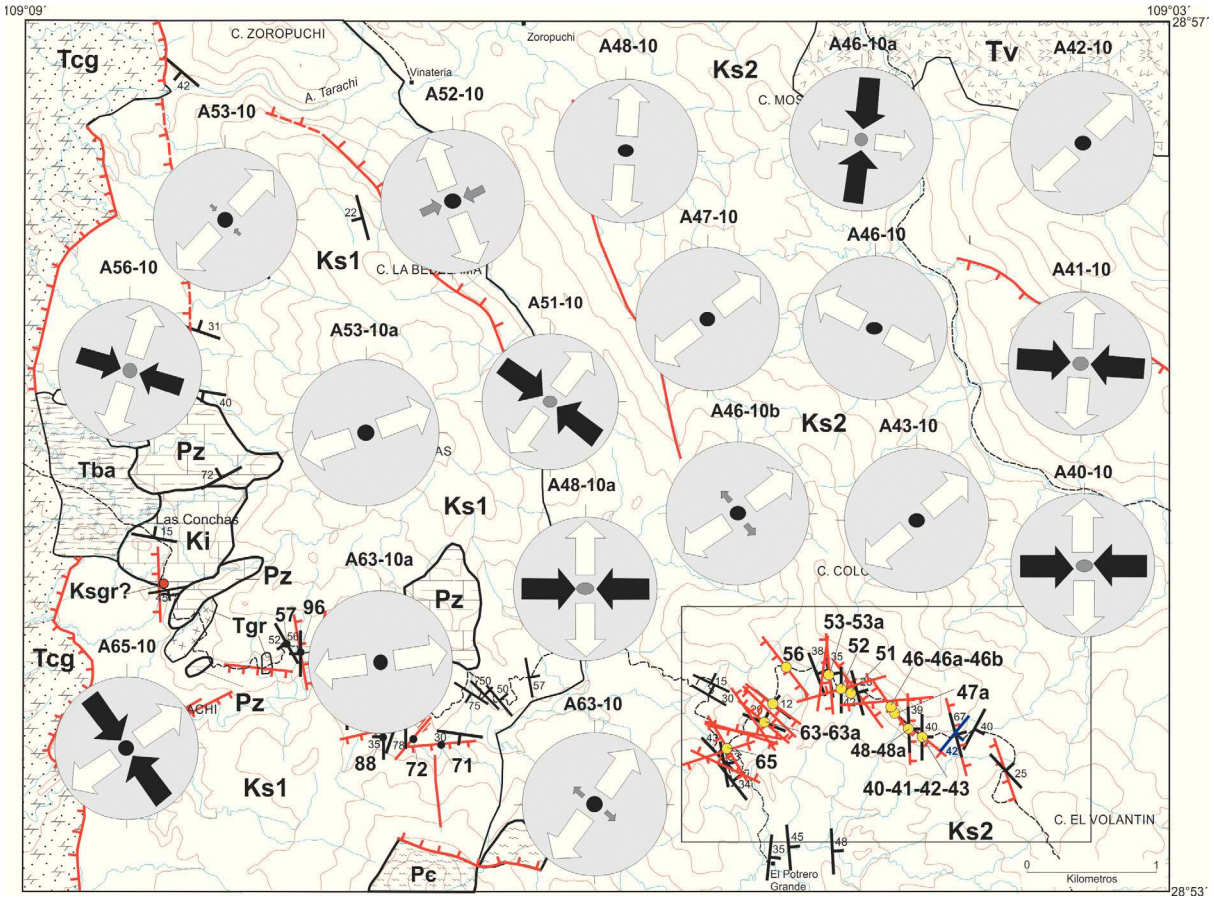

Figure 13. Orientation of the horizontal maximum and minimum stress in the El Potrero Grande Unit. The square shows the location of measured sites. Black arrow = S_1, white arrow = S_3. The central circle corresponds to S_1 when black and S_2 when gray.

the Aldama Platform continues to north-east Sonora as the Cananea High.

Other places with similar relationships in eastern Sonora near the study area are: Sierra La Madera, Lampazos and Sierra Los Chinos. In north-east Sonora along the margins of the Cananea High megaclasts were also identified at Sierra Los Ajos and Rancho San Antonio as well as in central Sonora in the Magdalena, Santa Ana and Tuape areas.

In the Arivechi-Tarachi area, east of Arivechi, two stress regimes have been recognized, one of pure extension and another with strike-slip displacement, affecting both Upper Cretaceous units exposed in the study area.

Prior to this study no paleostress data were reported for the area, but now we are able to compare the paleostress data with information reported by Rodríguez-Castañeda (2002) for the Rancho San Antonio area in north-eastern Sonora, i.e., an andesitic dike that registered NE-SW (S_3 = N058) and WNW-ESE (S_3 = N283) extensions at the arroyo Las Minas. In another locality towards the south of the previous locality at Rancho El Babiso, on rocks of the Baucarit Formation, S_3 is oriented NE-SW (S_h= 073). Other studies that can help with the interpretation of the Arivechi data include the method used by Angelier *et al*. (1981) in Baja, California Sur (around Santa Rosalia) and Angelier *et al*. (1985) at the Hoover Dam, Nevada, United States; they identify a chronology of events where the directions of a NE-SW to ENE-WSW extension are followed by an E-W to WNW-ESE extension with clockwise rotation. These studies suggest that such directions of extension are a product of a Basin and Range type normal faulting regime; even though it is possible to consider that the faults affecting the two Late Cretaceous units of the study area are associated with the Basin and Range event.

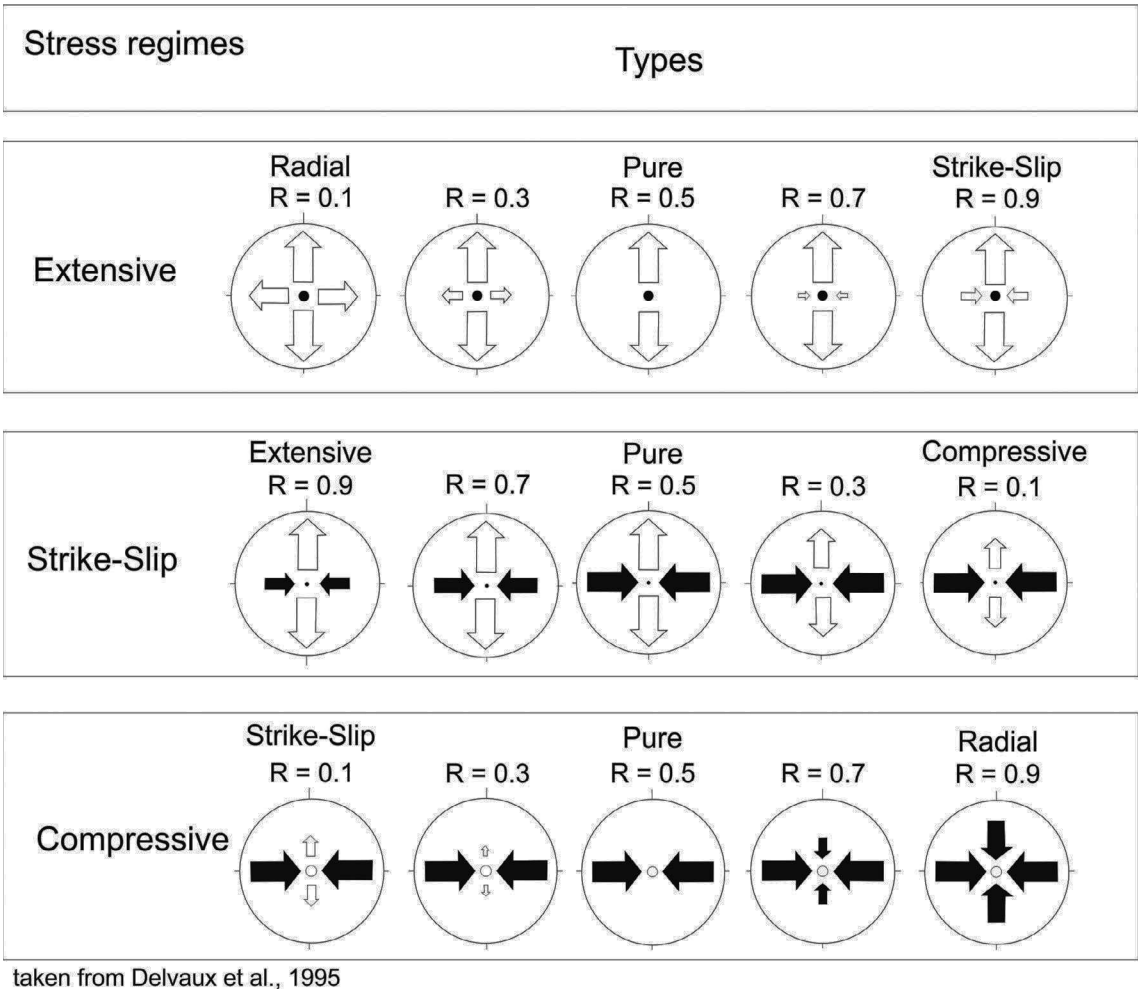

Figure 14. Types of stress regimes and their representation on a map. Arrows indicate the azimuth of horizontal stress axes, with their length according to relative stress magnitude, in base of the stress ratio *R*. White outward arrows indicate extensive stress axes and black inward arrows compressive stress axes. Vertical stress axes are symbolized by a solid circle for extensive regimes (S_1 vertical), a dot for strike-slip regimes (S_2 vertical) or an empty circle for compressive regimes (S_3 vertical).

The faults with a strike slip to oblique component movement are associated with the extensional regime and not with a strike-slip phase of deformation. That means that the direction of extension was not always perpendicular to the strike of the faults. Alternatively, along either side of the mass there must be strike-slip accommodation of movement by faults, reflecting the surface outcrop of the detachment plane as a tear fault. Tectonic compression, sensu stricto, was not detected. The package that constitutes the Cañada de Tarachi Unit is molded by deformational gliding structures. The identified ductile structures are related to the gliding tectonics of the monoliths. Assuming that compression existed in the area as a result of the Laramide deformation, we should observe structures, such as folds, that indicate a transport movement towards the north-east. Instead, the observed folding indicates a vergence towards the west and south-west. However, El Potrero Grande does not display these characteristics, indicating a different evolution of the tectonic environment.

Therefore, the development of basins and volcanism in central Sonora during the Triassic (Stewart and Roldán, 1991) and, later, the development of volcanism and the opening of basins during the Early and Middle Jurassic (Anderson and Nourse, 2005) mark an evolution associated with extension in a possibly thinned and warmed lithosphere. The sedimentation in the Upper Jurassic-Lower Cretaceous and Upper Cretaceous occurred under an extension environment, and indicates the completion of the evolution of the Mesozoic

basins that occurred before a period of stability and peneplanation in the Upper Cretaceous-Paleocene in north-west Sonora.

Conclusions

The volcano-sedimentary rocks of the Upper Cretaceous in the Arivechi comprise a sequence with sediment thickness of more than 6 km that was deposited in a back-arc basin. The stratigraphy of the Arivechi region consists of two Upper Cretaceous units: the Cañada de Tarachi Unit and the El Potrero Grande Unit. Both units show evidence of rapid denudation, magmatism and sedimentation developed in an extensional type regime environment.

An outstanding characteristic of the Cañada de Tarachi Unit is the presence of glided monoliths and blocks with tabular forms of diverse dimensions, from a few meters to several kilometers in length. Two of these megaclasts of granitic composition were dated: one at 76.0 ± 2.0 Ma by U/Pb zircon geochronology at the Cañada de Tarachi, and the second one at 69.57 ±0.48 Ma by $^{40}Ar/^{39}Ar$ step-heating of a K-spar along the Arivechi-Tarachi, road, interpreted as an emplacement and cooling age respectively, and a maximum age for the onset of erosion.

The recognized structures and the results of the paleostress study along with the stratigraphy demonstrate two periods of deformation. The first happened at the beginning of the Late Cretaceous, as shown by the presence of monoliths, blocks, and folds only in the Cañada de Tarachi Unit. The megaclasts were emplaced as slumps in soft sediments during successive mass movements derived from differential uplifts and associated gravitational gliding processes. Overall, the clasts deposited in the Arivechi basin are angular, unsorted monoliths, blocks and very coarse to fine slab. The back-arc Arivechi basin had to be a deep one, since a thick (6 km) detritus accumulation derived from a magmatic arc and basement source rocks can be observed. The origin of these uplifts was the result of several vertical regional movements of the Aldama Platform, as indicated by megaclasts interbedded in the sequence at different stratigraphic levels. The mechanism that originated uplifts suggests earthquakes, e.g., M 8, which occurred along the Denali fault in Alaska (Harp *et al*., 2003), triggered the mass-sliding and generation of megaclasts.

The folds are associated with movements along a synthetic extensional detachment, linked to the evolution of the gliding masses. The contact between megaclasts and the basal Cretaceous rocks are pervasively sheared because of the downslope transport. At the front and along the base of the megaclasts disintegration and a complex deformation associated with simple shear can be observed. The transport direction to W-SW is deduced from the kinematics of folds recorded in the Cretaceous Cañada de Tarachi Unit. Contractional structures are not observed in the El Potrero Grande Unit. Folds in the El Potrero Grande Unit are associated with the evolution of faults such as drag folds.

The second event was characterized by normal and strike-slip faults, which can be seen in both units. Paleostress analysis in the Arivechi region indicated that the area has undergone radial to NE-SW to NW-SE extension, and local compression in an E-W and NW-SE direction. The chronology of events identified suggests that the directions of extension NE-SW and ENE-WSW were followed by an E-W and WNW-ESE extension. This would indicate that the sequence of faulting went from NE-SW to ENE-WSW and later to WNW-ESE.

The presence of strike-slip faults is the result of a dominant extensional tectonic regime. It is thought that strike-slip faults were formed as a response to a main E-W and NW-SE compression stress, as a result of the reactivation of normal faults oriented NE-SW. Perhaps this reactivation occurred in faults during the sliding of masses and reactivated during the transformation of the tectonic regime during Miocene-Pliocene times. The NE-SW to WNW-ESE extension was in general the cause of the tilting towards the north-east of the Upper Cretaceous layers.

The structural analysis and paleostress reconstruction of the Arivechi area allow recognition of two major deformation events that can be related (1) to the Farallon oceanic lithosphere subduction under the North American plate and the opening of the back-arc basin and (2) a stress field characterized by extension related to the right lateral displacement between the Farallon and North American plates. In both Late Cretaceous units only extension is observed. This extension can be divided into two periods. The first one, during Lower Cretaceous times, is recorded in the structures and megaclasts observed at the Cañada de Tarachi Unit. These structures are the result of differential uplifts which caused the gravitational gliding masses and contractional structures. The second one is related to the basin and range Cenozoic normal faulting observed in both units. No evidence

of compressional tectonics is reported in this work.

The tectonic history of the Aldama Platform and the Cananea High is based upon their lithological constitution and structural heterogeneous basement, which are precursors of the faulting initiated at the end of the Early Cretaceous. Both structural elements were possibly active at least from the Jurassic (Aldama Platform) to the late Early Cretaceous in the light of the characteristics identified in the rocks involved in the sliding processes.

Acknowledgments

This research project was funded by a UNAM-PAPPIT Grant, number 22-IN103710. Grinding of samples and preparation of thin sections were performed by Pablo Peñaflor and Aime Orci, respectively, from the Estación Regional del Noroeste, Instituto de Geología, UNAM. U/Pb dating was completed at the Centro de Geociencias, UNAM, where Carlos Ortega-Obregón and Ofelia Pérez-Arvizu carried out the laboratory analysis. Identification of fossils in the conglomerate was performed by Rogelio Monreal from the Department of Geology of the University of Sonora at Hermosillo.

References

Allaby A., Allaby M., 1999, A Dictionary of Earth Sciences: Oxford University Press, 619 pp.

Almazán-Vázquez E., 1989, El Cámbrico-Ordovícico de Arivechi, en la región centro oriental del Estado de Sonora, *Revista Mexicana de Ciencias Geológicas,* 8, 1*, 58-66.*

Andersen T., 2002, Correction of common lead in U–Pb analyses that do not report 204Pb, *Chemical Geology,* 192, *59-79*.

Anderson T.H., Nourse J.A., 2005, Pull apart basins at releasing bends of the sinistral Late Jurassic Mojave-Sonora fault system, *in*: Anderson, T.H., Nourse, J.A., McKee, JW., Steiner, M.B. (eds.), The Mojave-Sonora megashear hypothesis: Development, assessment, and alternatives: *Geological Society of America, Special Paper,* 393, 97-122.

Angelier J., 1994, Fault slip analysis and paleostress reconstruction, in Hancock, P.L., (ed.), Continental Deformation. Pergamon, Oxford, 101-120 pp.

Angelier J., Colletta B., Anderson R.E., 1985, Neogene paleostress changes in the Basin and Range: A case study at Hoover Dam, Nevada-Arizona, *Geological Society of America Bulletin,* 96, 3*, 347-361*.

Angelier J., Colletta B., Chorowicz J., Ortlieb L., Rangin C., 1981, Fault tectonics of the Baja California Peninsula and the opening of the Sea of Cortez, Mexico, *Journal of Structural Geology,* 3, 4, 347-357.

Angelier J., Mechler P., 1977, Sur une méthod graphique de recherché des contraintes principal ségalement utilisable en tectonique et en seismologie: la méthode des diedresdroits. *Bulletin de la Société Geologique de France,* 7, 19, *1309-1318.*

Bailey R.H., Skehan J.W., Dreier R.B., Webster M., 1989, Olistostromes of the Avalonian terrane of southeastern New England, in Horton, J.W., Rast, N. eds. Mélanges and Olistostromes of the U.S. Appalachians: *Geological Society of America Special Paper* 228, p. 93-112.

Bartolini C., 1993, Fragments of the lower Cretaceous Chihuahua´s Aldama platform in eastern Sonora, Mexico: *Cordilleran Section, Abstracts with Programs, Geological Society of America,* 25, 5, 7.

Blair T.C., McPherson J.G., 1999, Grain-size and textural classification of coarse sedimentary particles. *Journal of Sedimentary Research,* 69, 1, 6-19.

Carrasco-Velázquez B., 1977, Albian sedimentation of submarine autochthonous and allochthonous carbonates, east edge of the Valle-San Luis Potosí platform, Mexico, in Cook, H.E., Enos, P., eds., Deep-Water Carbonate Environments, SEPM Special Publication 25, 263-272.

Conaghan P.J., Montjoy E.W., Edgecombe O.R., Talent J.A., Owen D.E., 1976, Nubrigyn Algal Reef (Devonian), eastern Australia: allochthonous blocks and megabreccias. *Geological Society of America Bulletin,* 87, 515-530.

Cook H.E., McDaniel P.N., Mountjoy E.W., Pray L.C., 1972, Allochthonous carbonate debris flows at Devonian bank ("reef") margins, Alberta, Canada. *Association of Canadian Petroleum Geologists Bulletin,* 20, 439-497*.*

Delvaux D., 1993, The TENSOR program for reconstruction examples from the East African and the Baikal rift zones: Terra Abstracts. *Abstract Supplement 1 to Terra Nova,* 5, 216.

Delvaux D., Moeys R., Stapel G., Melkinov A., Ermikov V., 1995, Paleostress reconstructions and geodynamics of the Baikal region, Central Asia, Part I. Palaeozoic and Mesozoic pre-rift evolution. *Tectonophysics,* 252, 61-101.

Díaz A., Monreal R., 2008, La Formación Los Picachos en la Sierra de Los Chinos, Sonora, México. *Boletín de la Sociedad Geológica Mexicana,* 60, 1, 111-120.

Fernández-Aguirre, M.A., Almazán-Velázquez E., 1991, Geología de la carta Arivechi (H12D56): Secretaría de Fomento Industrial y Comercio del Estado de Sonora, Dirección General de Fomento Minero, Mapa.

Fernández-Aguirre M.A., Grijalva-Haro A.S., Estrada-Cubillas R., 1995, Carta Geológica Sahuaripa, escala 1: 50,000: Secretaría de Desarrollo Económico y Productividad, Gobierno del Estado de Sonora. Mapa.

Flinn D.L., 1977, Geology of Cerro Macho area, Sonora, Mexico [Master thesis]. Flagstaff, Northern Arizona University, 73 pp.

García y Barragán J.C., Rodríguez-Castañeda J.L., 1996, Tectonic significance of Late Cretaceous conglomerates in north-central Sonora, México. *Geological Society of America, Abstracts with Programs,* 28, 7, 115.

González-León, 1988, Estratigrafía y geología estructural de las rocas sedimentarias Cretácicas del área de Lampazos, Sonora. *Universidad Nacional Autónoma de México, Instituto de Geología,* 7, 148-162.

Grajales-Nishimura J.M., Terrel D., Torres-Vargas R., Jacques-Ayala C., 1990, Late Cretaceous synorogenic volcanic/sedimentary sequences in eastern Sonora, Mexico. *Geological Society of America, Abstracts with Programs,* 22, 3, 26.

Haenggi W.T., 2002, Tectonic history of the Chihuahua Trough, Mexico and adjacent USA, Part II Mesozoic and Cenozoic. *Boletín Sociedad Geológica Mexicana, LV,* 1, 38-94.

Harp E.L., Jibson R.W., Kayen R.E., Keefer D.K., Sherrod B.L., Carver G.A., Collins B.D., Moss R.E.S., Sitar N., 2003, Landslides and liquefaction triggered by the M 7.9 Denali fault earthquake of 3 November 2003. *AUGUST GSA TODAY,* 4-10.

Heck F., Speed R., 1987, Triassic olistostrome and shelf-basin transition in the western Great Basin: paleogeographic implications. *Geologic Society of America Bulletin.* 99, 539-55l.

Herrera S., Bartolini C., 1983, Geología del área de Lampazos Sonora [Tesis Licenciatura]. Universidad de Sonora, Hermosillo, Sonora, México, p.120.

Heubeck C., 1992, Sedimentology of large olistoliths, southern Cordillera Central, Hispaniola. *Journal of Sedimentary Petrology,* 62, 3, 474-482.

Himanga J.C., 1977, Geology of Sierra Chiltepín, Sonora, México [Master thesis]. Flagstaff, Northern Arizona University, p.78.

Johns D.R., Mutil E., Rosell J., Séguret, M., 1981, Origin of a thick, redeposited carbonate bed in Eocene turbidites of the Hecho Group, south-central Pyrenees, Spain. *Geology,* 9, 161-164.

King R.E., 1939, Geological reconnaissance in the northern Sierra Madre Occidental of Mexico. *Geological Society of America, Bulletin,* 50, 1625-1722.

Ludwig K., 2008, Manual for Isoplot 3.7. Berkeley Geochronology Center Special Publication No. 4, rev. August 26, 77.

Ludwig K.R., Mundil R., 2002, Extracting reliable U–Pb ages and errors from complex populations of zircons from Phanerozoic tuffs. Goldchmidt Conference Abstracts 2002. *Geochim. Cosmochim. Acta,* 66, 15A, A463.

McKee M.B., 1991, Deformation and stratigraphy relationships of mid-Cretaceous mass gravity slides of a marine basin in Sonora, Mexico [PhD thesis]. Pittsburgh, PA, University of Pittsburgh, p. 286.

McKee M.B., Anderson T.H., 1998, Mass gravity deposits and structures in the Lower Cretaceous of Sonora, Mexico. *Geological Society of America Bulletin,* 110, 1516-1529.

McKee J.W., McKee M.B., Anderson T.H., 2005, Mesozoic formation, mass gravity sedimentation and inversion in northeastern Sonora and southeastern Arizona, in

Anderson, T.H., Nourse, J.A., McKee, J.W., Steiner, M.B., eds., The Mojave-Sonora Megashear Hypothesis: Development, Assessment, and Alternatives: Geological Society of America Special Paper 393, pp. 481-507.

Minjárez-Sosa I., Palafox J.J., Torres Y., Martínez J.A., Rodríguez B., 1985, Consideraciones respecto a la estratigrafía y estructura del área de Sahuaripa - Arivechi. *Universidad de Sonora, Boletín del Departamento de Geología,* 2, 1-2, 90-105.

Monreal R., 1995. Las facies marinas (Aptiano-Albiano) del Grupo Bisbee y cronocorrelativas en Sonora: México, Hermosillo, Son. *Universidad de Sonora, Boletín del Departamento de Geología,* 12, 1, 65-78.

Monreal R., 1996, Cretaceous stratigraphy and structure of the Sierra Grande, northeastern Chihuahua, in Jacques-Ayala, C., González-León, C.M., Roldán-Quintana, J., (eds.), Studies on the Mesozoic of Sonora and Adjacent areas: Boulder, Colorado. *Geological Society of America, Special Paper,* 301, 167-178.

Monreal R., Longoria J.F., 2000, Lower Cretaceous rocks of Sierra de Los Chinos, east-central, Sonora, Mexico. *Geofísica Internacional,* 39, 4, 309-322.

Naylor M.A., 1982, The Casanova Complex of the northern Apennines: a mélange formed on a distal passive continental margin. *Journal of Structural Geology,* 4, 1-18.

Onstott T., Peacock M., 1987, Argon retentivity of hornblendes: A field experiment in a slowly cooled metamorphic terrane. *Geochimica et Cosmochimica Acta,* 51, 2891-2903, doi:10.1016/0016-7037(87)90365-6.

Palafox J.J., Martínez J.A., 1985, Estratigrafía del área de Arivechi, Sonora. *Universidad de Sonora, Boletín del Departamento de Geología,* 2, 1-2, 30-56.

Palafox J.J., Minjárez J.L., Pubellier M., Rascón B., 1984, Sobre la presencia de rocas del Paleozoico Superior en el área de Arivechi, Sonora, México. *Universidad de Sonora, Boletín del Departamento de Geología,* 1, 1, 60-62.

Prior D.B., Bornhold D.B., Coleman J.M., Bryant W.R., 1982, Morphology of a submarine slide, Kitimat Arm, British Columbia. *Geology,* 10, 58S-592.

Pubellier M., 1987, Relations entre domaines cordillérain et mésogéen au nord du Mexique; étude géologique de la vallé de Sahuaripa, Sonora central [PhD thesis]. Paris, Université de Paris 6, 219 p.

Ramírez-M J.C., Acevedo-C. F., 1957, Notas sobre la geología de Chihuahua. *Boletín de la Asociación Mexicana de Geólogos Petroleros,* IX, 9-10, 583-770.

Rangin C., 1977, Tectónicas sobrepuestas en Sonora septentrional. *Universidad Nacional Autónoma de México, Boletín del Instituto de Geología,* 1, 44-77.

Rangin C., 1982, Contribution à l´étude géologique du Systeme Cordillérain du nord-ouest du Mexique [PhD thesis]. Paris, Université Pierre et Marie Curie, 588 p.

Roddick J., 1983, High precision intercalibration of 40Ar-39Ar standards. *Geochimica et Cosmochimica Acta,* 47, 887-898, doi:10.1016/0016-7037(83)90154-0.

Rodríguez-Castañeda J.L., 2002, Tectónica Cretácica y Terciaria en la margen suroeste del Alto de Cananea, Sonora, Norte Central [PhD Thesis]. México, D.F., Universidad Nacional Autónoma de México, 217 p.

Servicio Geológico Mexicano, 2008, Carta Geológica-Minera del Estado de Sonora, escala 1:500,000.

Slama J., Kosler J., Condon D., Crowley J., Gerdes A., Hanchar J., Horstwood M., Morris G., Nasdala L., Norberg N., Schaltegger U., Schoene B., Tubrett M., Whitehouse M.J., 2008, Plešovice zircon — A new natural reference material for U–Pb and Hf isotopic microanalysis. *Chemical Geology,* 249, 1-35, doi: 10.1016/j.chemgeo.2007.11.005.

Solari L., Gómez-Tuena A., Bernal J., Pérez-Arvizu O., Tanner M., 2010, U-Pb Zircon geochronology with an integrated LA-ICP-MS microanalytical workstation: Achievements in precision and accuracy. *Geostandards and Geoanalytical Research,* 34, 1, 5-18.

Solari L.A., Tanner M., 2011, UPb. age, a fast data reduction script for LA-ICP-MS U-Pb geochronology. *Revista Mexicana de Ciencias Geológicas,* 28, 1, 83-91.

Spalletti L.A., 2006, Curso Sedimentología. Facultad de Ciencias Naturales y Museo, UNLP.

Steiger R., Jäger E., 1977, Subcommission on geochronology. *Earth and Planetary Science Letters,* 36, 359-362, doi:10.1016/0012-821X(77)90060-7.

Stewart J.H., Amaya-Martínez R., Palmer A.R., 2002, Neoproterozoic and Cambrian strata of Sonora Mexico: Rodinian supercontinent to Laurentian Cordilleran margin, in Barth, A.P. (ed.), Contributions to crustal evolution of the southwestern United States: *Geological Society of America, Special Paper,* 365, 5-48.

Stewart J.H., Roldán-Quintana J., 1991, Upper Triassic Barranca Group, non-marine and shallow-marine rift-basin deposits of northwestern Mexico. *Geological Society of America, Special Paper,* 254, 19-36.

Teale T.C, Young J.R., 1987, Isolated olistoliths from the Longobucco Basin, Calabria. Southern Italy, in Leggett, J.K., Zuffa, G.G., eds., Marine Clastic Sedimentology. Graham and Trotman, London, pp. 15-88.

Tera F., Wasserburg G., 1972, U-Th-Pb systematics in three Apollo 14 basalts and the problem of initial Pb in lunar rocks. *Earth and Planetary Science Letters,* 14, 281-304.

Weber R., Ceballos-Ferriz S., López-Cortés A., Olea-Franco A., Singer-Sochet S., 1979, Los estromatolitos del Precambrico tardío de los alrededores de Caborca, Estado de Sonora, parte I; Reconstruccion de Jacutophyton Shapovalova e interpretación paleoecologica preliminar. *Universidad Nacional Autónoma de México, Instituto de Geología, Revista,* 3, 1, 9-23.